HHS Public Access

Author manuscript

Nature. Author manuscript; available in PMC 2025 July 08.

Published in final edited form as:

Nature. 2024 December ; 636(8042): 361–367. doi:10.1038/s41586-024-08175-5.

Sacrificial capillary pumps to engineer multiscalar biological forms

Subramanian Sundaram[1,2,*], **Joshua H. Lee**[1], **Isabel M. Bjørge**[1,3], **Christos Michas**[1,4], **Sudong Kim**[1,2], **Alex Lammers**[1,2], **João F. Mano**[3], **Jeroen Eyckmans**[1,2], **Alice E. White**[4,5], **Christopher S. Chen**[1,2,*]

[1]Biological Design Center and Department of Biomedical Engineering, Boston University, Boston, MA, USA

[2]Wyss Institute for Biologically Inspired Engineering, Harvard University, Boston, MA, USA

[3]Department of Chemistry, CICECO, University of Aveiro, Campus Universitário de Santiago, 3810-193 Aveiro, Portugal

[4]Department of Mechanical Engineering, Boston University, Boston, MA, USA

[5]Department of Physics and Department of Material Science and Engineering, Boston University, Boston, MA, USA

Abstract

Natural tissues are composed of diverse cells and extracellular materials whose arrangements across multiple length scales—from sub-cellular lengths[1] (~μm) to whole organ-scale[2] (~cm)—regulate biological functions. Methods that aim to engineer tissue structures have progressed in generating large constructs, e.g., through stereolithography[3] and nozzle-based bioprinting[4,5], and separately in subcellular patterning through subtractive processes like photoablation[6–8]. Despite these advances, additive bioprinting technologies cannot readily achieve sub-nozzle/voxel features[9], and subtractive photoablation is restricted to small volumes due to prohibitive heat generation and time[10]. Building across multiple length-scales at once with the constraints of temperature-sensitive and water-based soft biological matter has emerged as a critical challenge, leaving large classes of biological motifs—such as hierarchical vascular and ductal trees with continually changing calibers—inaccessible with current technologies[11,12]. Here we use gallium-

* subras@bu.edu, chencs@bu.edu.

Author contributions

S.S. and C.S.C. conceived and designed the research. S.S. designed the process, wrote custom code, analyzed data, and was involved in all aspects of the work. S.S., J.H.L. and I.M.B. performed experiments. S.S. and C.M. printed two-photon direct writing molds under A.E.W.'s supervision. S.K. advised on cell experiments. A.L. performed multiphoton microscopy optimization. J.F.M. co-supervised I.M.B.'s work. S.S., J.E., and C.S.C. wrote the manuscript. All authors discussed and contributed to the manuscript.

Competing interests

A patent application (U.S. Appl. No. 18/422,963) has been filed by Boston University based on this work. C.S.C. is a founder and owns shares of Innolign Biomedical, a company that is developing engineered organ models for pharmaceutical research and development, and Satellite Biosciences, a company that is developing cell-based therapies. The other authors declare that they have no competing interests.

Materials & Correspondence

Correspondence and requests for materials should be addressed to S.S. (subras@bu.edu) and C.S.C. (chencs@bu.edu).

Code availability. Blender/Python code used to computationally generate vascular trees, OpenSCAD code to generate CAD designs, and MATLAB code to analyze images are available from the corresponding authors on request.

based engineered sacrificial capillary pumps for evacuation (ESCAPE) during molding and demonstrate the ability to generate multiscalar structures in soft natural hydrogels achieving both cellular-scale (<10 μm) and mm-scale features. Decoupling the biomaterial of interest from the process of constructing the geometry allows us to utilize non-biocompatible tools to create the initial geometry. As an exemplar, we fabricated branched, cell-laden vascular trees in collagen, transitioning from ~300 μm arterioles down to the microvasculature (~10× smaller). The same approach can micropattern the inner surface of vascular walls with topographical cues to orient cells in 3D and engineer fine structures such as vascular malformations. ESCAPE molding enables the fabrication of multiscalar forms in soft biomaterials, laying the foundation for building a wide range of tissue architectures previously inaccessible in vitro.

An ever-expanding toolkit of printing technologies is being used to build complex 3D shapes[13] ranging from the nanoscale[14] to architectural scales[15]. Yet only a minuscule subset of these processes function in environments that are safe for cells and natural extracellular matrices (ECMs), or yield scaffolds suitable for cell culture. Emerging fabrication technologies like two-photon lithography can directly print complex 3D shapes with hydrogels[16], but such technologies cannot build these structures with natural ECMs and are limited to specially tuned materials, small print volumes and ultralow throughput. To tackle the current bottleneck in engineering multiscalar biological structures, we sought to develop molding approaches that work with a range of natural ECMs (like collagen and fibrin). Molding allows copying 3D shapes into soft natural ECMs starting from complex molds, independent of how those molds were originally formed[17] in contrast to bioprinting approaches that build shapes from scratch. Notably, despite the progress of sacrificial gel printing methods[18], these techniques do not achieve μm-scale resolution, sharp corners, or abruptly changing geometries due to the nozzle-based, liquid deposition scheme and the fragility, surface tension and slow kinetics inherent to the printed sacrificial gel. As such, successful templating strategies would expand the range of 3D-printing processes (including non-biocompatible processes) used to produce molds for the fabrication of biological materials. Sacrificial template-based molding of soft ECMs has been extensively explored with both soft[19] and rigid templates[20] but a single approach to mold both cellular-scale (<10 μm) and millimeter scale 3D features is yet to be demonstrated. Photolithographic templating methods[21] that achieve a broad range of in-plane dimensions (and typically a single out-of-plane thickness) have been useful to mold 2.5D geometries (i.e., without overhangs) but not freeform 3D structures. Fundamentally, the challenge stems from the competing mechanical requirements of the molding process: rigid templates that mold small features with high geometric fidelity, once the biological material has set, are difficult to remove without destroying the surrounding soft material (especially for freeform 3D molds) whereas soft templates such as sacrificial gels that are easily removed do not replicate microscale features faithfully.

We reasoned that gallium is an ideal templating material to copy multiscalar biological structures into natural ECMs as: (1) its melting point (~29.8 °C) is near cell culture temperatures enabling its use both as an injectable liquid[22–24]and resilient solid casting material[25] as well as a low viscosity liquid[22] for demolding in the presence of natural ECMs, and (2) its tunable surface oxide[26] enables the use of capillary forces in the

demolding process, conferring both spatial control and the ability to evacuate complex features hierarchically (as Laplacian pressure is inversely proportional to feature size). The surface oxide of gallium is amphoteric and is removed by both acids and bases, however, the high concentrations typically used (~ 1M HCl or 1M NaOH)[27] degrade natural ECMs rapidly. From the Pourbaix chart of the gallium-water system[28], we hypothesized that milder bases will gradually remove the surface oxide without affecting natural ECMs and would lead to controlled capillary pumping of liquid gallium in water-based environments including hydrogels. This was further supported by experiments showing that Ga can be dislodged easily from hydrogel surfaces as compared to removal from PDMS (see Methods), making oxide removal with milder bases practical (Supplementary Fig. 1; Supplementary Video 1).

To investigate this, we assembled gallium filaments (150 μm diameter) to span across 6 mm-wide chambers and polymerized collagen around the filaments (Fig. 1a). Upon melting the filament (see Methods) and removing its surface oxide with NaOH (high interfacial tension state), the geometric asymmetry between the two filament ends results in a Laplacian pressure difference that drives unidirectional capillary flow. At NaOH concentrations of 100 mM (Fig. 1b; Supplementary Video 2) or 50 mM (Supplementary Video 3), liquid Ga rapidly extracts itself from the gel (typically < 1 min). An abrupt change in surface tension results in inconsistent evacuation, at times, fragmenting the liquid plug into multiple pieces. With 20 mM and 10 mM NaOH, however, the gradual removal of the surface oxide ensured that liquid gallium consistently evacuated as a single non-fragmented droplet (Supplementary Video 4 & 5); the resulting conduit through the collagen gel is visualized with colored beads (inset Fig. 1b). To assess the dimensional stability of collagen, we performed second harmonic generation (SHG) imaging of preformed collagen cavities after exposure to different NaOH concentrations. Sharp boundaries and overall dimensional accuracy were preserved after 30 min exposure to NaOH at concentrations 20 mM and below (Extended Data Fig. 1a–1c) but not at 50 mM NaOH where we observed substantial dimensional changes and blurring of the edges. At 100 mM NaOH, the boundaries of the gel could no longer be identified clearly. Furthermore, SHG imaging of bulk collagen gels revealed that the overall fibrillar architecture and intensity of collagen were not substantially altered at NaOH concentrations up to 20 mM (30 min exposure) but were affected at 50 mM and above (Extended Data Fig. 1d–1e). Based on these collective results, we typically use 10 mM or 20 mM NaOH in further experiments.

We next describe the theoretical considerations for efficient unidirectional capillary pumping of liquid gallium (Fig. 1c). Pure gallium (without its native oxide) exhibits a ~180° contact angle in water-based environments due to its high surface tension[29] (~708 mN/m). The local Laplace pressure at the gallium-water interface is $2\gamma/r$ where γ is the interfacial tension, and r is the principal radius of curvature. Laplace pressure differentials result from geometric asymmetries[30] (case I in Fig. 1c), surface tension gradients (case II) or from a droplet exiting a constricted region (case III; a special case of I). Liquid plugs in cases I and II undergo unidirectional flow when constrained by rigid walls that counter the forces exerted by gallium. When surrounded by soft gels, the internal pressure of gallium can dominate and allow it to form a spherical droplet, deforming the gel (termed elastocapillarity[31,32]) and entrapping itself (Supplementary Fig. 2a). To be effectively rigid to prevent this entrapment,

the elastic modulus of the surrounding material must be larger than $3\gamma/r$ (Supplementary Fig. 2b; full derivation in Supplementary Information); natural ECMs are softer than this threshold for values of r less than the capillary length of Ga (Supplementary Fig. 2c). Thus, in contrast to surrounding matrices such as PDMS (modulus ~ MPa), to evacuate gallium reliably from within soft ECMs (moduli ~100 Pa), the lowest Laplacian pressure must be maintained outside the structure being evacuated (as in case III of Fig. 1c). We achieve this practically with a bulb of gallium at the collecting end of the mold.

The ESCAPE molding process for forming 3D structures in ECMs is illustrated in Fig. 1d using the Stanford Bunny as an example (see Methods for process details and Supplementary Information and Supplementary Fig. 3 for the general design principles). First, the intended structure is designed and printed (step I) and a negative copy is made with a soft elastomer (step II). Here we primarily used a commercial two-photon direct write system to form the mold (Extended Data Fig. 2a) and crosslinked polydimethylsiloxane (PDMS) around the mold to form negatives (Extended Data Fig. 2b); note that the process is agnostic to how the mold and negative structure are fabricated. Liquid gallium is filled and solidified in the cavity, and subsequently removed (or selectively etched) to generate the cast (step III). The gallium cast is then assembled into a device (Extended Data Fig. 2c) and the desired soft material is polymerized around it (step IV). Finally, gallium is liquified and evacuated using capillary forces (step V); phase contrast images of the mm-scale Stanford Bunny cavity are in Extended Data Fig. 2d. The empty cavity was used as a 3D cell culture substrate wherein human endothelial cells (ECs) were seeded to form a confluent lining to illustrate the final biological form of interest. Depth-coded projections of the cell nuclei are in Fig. 1e (top-view) and Extended Data Fig. 2e (front-view); Extended Data Fig. 2f shows cellular proteins F-actin (cytoskeleton) and VE-cadherin (cell-cell junctions). To evaluate patterning fidelity, we compared the collagen cavity (before cell seeding) with the original design (see Extended Data Fig. 2g) and observed that fine features such as the ear tips (~50 μm) and the overall 3D body shape (~1 mm) were well replicated in the collagen gel.

Some closed topologies like tubes that split and merge (e.g., top design in Extended Data Fig. 3a) provide a distinct challenge for the ESCAPE process as the liquid gallium must break at each loop to be extracted (Extended Data Fig. 3b). Gallium was found to break reliably if the Laplace pressure of the collecting droplet (far left) is lower than the driving Laplace pressure. This is critical for evacuating topologies that branch and remerge as the driving Laplace pressure drops at such junctions, as one principal curvature approaches 0. Even dead-ended sections are evacuated reliably in hydrogels (in contrast to non-porous surrounding materials) as NaOH reaches the terminal sections of dead-ends through the bulk (Extended Data Fig. 3c and Supplementary Video 6).

In addition to collagen, we used fibrin and agarose to demonstrate that the ESCAPE process is agnostic to the surrounding hydrogel materials (see Extended Data Fig. 3d–3e and Supplementary Video 7–9). We next sought to understand if gallium exposure to the hydrogels would lead to cytotoxicity when cells are cultured post gallium removal. To directly assess this, we cultured human ECs in physical contact with gallium droplets for 4 days (Extended Data Fig. 3f). On performing a live-dead assay (see Methods), we did not observe increased cell death, and furthermore, the cells spread and grew directly on

top of the gallium droplet (Extended Data Fig. 3g). Therefore, we expect that any potential traces of gallium remnant from the ESCAPE process (if present post long-term washing; see Methods) to not be cytotoxic. We quantified the remnant Ga residues on collagen surfaces post ESCAPE to be < 0.2% (atomic conc.) through energy dispersive spectroscopy (EDS) and ~0.2 % areal coverage of particulates through SEM imaging (see Supplementary Fig. 4 & Methods).

To demonstrate the versatility of our fabrication approach, we focus on vasculature as a use case as the multiscalar diversity of vascular forms has been well established as a fabrication challenge[11,12]. First, we developed a theoretical framework for the evacuation of natural hierarchical vascular networks through sacrificial capillary pumping (details in the Supplementary information and Supplementary Fig. 5); scaling relationships for capillary pressure, network impedance, evacuation flow rates and velocities show that natural branching laws favor liquid gallium evacuation through capillary pumps.

To establish a comparative baseline with prior needle molding approaches used to form linear blood vessels[33], we seeded endothelial cells (ECs) into 150 μm-sized ESCAPE-molded tubes and cultured them under flow (see Extended Data Fig. 4a, 4b and Methods). The functionality of these vessels as assessed by the endothelial barrier to transmural leakage is in Supplementary Fig. 6 (see Supplementary Video 10 and Methods). Immunofluorescence images show a confluent layer of cells that orient towards the longitudinal axis. In smaller 60 μm-sized vessels, fewer ECs are necessary to cover the vessel (Fig. 2a shows maximum projections of half a vessel). To assess the smallest dimensions of vessels that are reliably covered by ECs, we designed a device tapering from 150 μm to 20 μm (~size of an EC in suspension). ECs completely cover sections larger than 25 μm (Extended Data Fig. 4c) but began showing incomplete coverage at around 20 μm—the typical limit for seeding ECs in our devices.

In sinusoidal vessels (see Extended Data Fig. 4d, Fig. 2b), cells cover both the linear and curved sections uniformly and align along the vessel axis. Uniform cell coverage is achieved in vessel architectures with symmetric branching (Fig. 2c) and asymmetric branching with dead ends (Extended Data Fig. 2e). We increased the complexity of vessels with a bidirectional (3, 2) branching design that branches from a 150 μm parent vessel into 3 daughter vessels that each bifurcate and rejoin and whose vessel calibers are based on Murray's Law[34,35]; see Extended Data Fig. 4g and discussion on the trifurcation design considerations in Supplementary Information and Supplementary Fig. 3d. The final dimensions closely match the intended design with only minor differences arising from EC-generated contractile forces that reduce vessel diameters (Extended Data Fig. 4h and 4i). Liquid gallium is evacuated successfully even when constrictions are added to the smallest vessels of this design (Extended Data Fig. 4j).

Complex interlocking geometries cannot be molded in a single mold nor be printed with nozzle-based methods in one piece, whereas multicomponent molding and printing in multiple passes result in interface defects. We considered if traditionally "non-moldable" designs such as an overhand knot are achievable using the ESCAPE process relying on the high surface tension of Ga. To make such geometries moldable, we designed thin continuous

walls supporting the entire geometry (Extended Data Fig. 5a) while simultaneously ensuring that the wall thickness prevents high surface tension Ga from filling the supports (Extended Data Fig. 5b). The original knot and the printed knot designs are shown in Extended Data 5c; PDMS negative and Ga casts in Extended Data Fig. 5d–5f. The endothelialized overhand knot formed in collagen illustrates the ability to generate topologically complex features using ESCAPE molding (Fig. 2d, and Extended Data Fig. 5g and 5h).

In addition to overall blood vessel architecture, ESCAPE allows high resolution control of fine vascular forms. To demonstrate this, we fabricated vascular malformations or spherical blebs extending out from the cylindrical wall with different offsets as shown in Fig. 2e and Extended Data Fig. 6a. These images highlight that the ESCAPE process yields smooth collagen surfaces (without large ridges; Extended Data Fig. 6b) and sharp boundaries (collagen SHG slice in Extended Data Fig. 6c). Furthermore, ESCAPE molding enables direct control of local EC alignment within blood vessels—a well-established factor of vascular health and physiology[36]—which has been challenging to achieve in 3D structures in soft natural ECMs. We introduced periodic microscale topographical cues in the form of ridges (width and height 10 μm) lining the inner wall of the vessel, at different orientations θ with respect to the vessel axis (Fig. 2f & Extended Data Fig. 6e). These topographical cues drove cell alignment to predefined angles with precise control (histograms and images are in Extended Data Fig. 6f; see Methods).

To highlight the capabilities in fabricating hierarchical architectures, we designed a range of branching vascular forms. First, we designed a hierarchical tree with 5 levels of branching where each level consists of a parent branching into two dead-ended and one through branch (Fig. 3a and Extended Data Fig. 7a). The design then tapers down to a single tube (~30 μm), overall, a 10× reduction in vessel caliber—down from 300 μm; see printed designs and Ga cast in Extended Data Fig. 7b, 7c. The vessel calibers post cell seeding closely follow the original design (Extended Data Fig. 7d). Next, we designed a branching tree where every vessel bifurcates into identical vessels that are all perfusable, branching from one inlet into 32 outlets (Fig. 3b & Extended Data 7e, 7f; see cell alignments in Supplementary Fig. 7).

The previous vascular trees with calibers obeying Murray's law are orderly in a manner natural vessels rarely are. Inspired by the effectiveness of computational space filling algorithms, we developed a custom version of the space colonization algorithm[37,38] to design more life-like vasculature (see Methods for full description). Briefly, N virtual cells distributed randomly in a bounded space attract the growing branches of a tree until the branches come within a predefined distance (called vessel-cell distance, or VCD). Extended Data Fig. 8 shows dead-ended trees to nourish a 4 mm × 4 mm area generated using distinct design parameters that control the number and density of vessels, their tortuosity and overall alignment. Here, we fabricated one design (N = 1000, VCD = 100 μm) terminating in 99 dead-ended branches (see Fig. 3c and Supplementary Video 11); elastomer negative and Ga cast are shown in Extended Data Fig. 9a. The cell laden vascular tree is shown in Fig. 3d and Extended Data Fig. 9b; closeups show branching regions and dead ends. We next synthesized a vascular tree using marginal growth where the boundary to be vascularized is progressively expanded (to simulate organ growth) and fabricated the final design (see Fig. 3e, Extended Data Fig. 10a and 10b). In addition to these mostly planar branching

architectures, fully 3D hierarchical branching vascular trees following Murray's Law can be made with ESCAPE as shown in Fig 3f and Extended Data Fig. 10c–10f (see Methods).

Although our demonstrations have so far focused on vasculature, ESCAPE molding is applicable to other organotypic forms and engineered tissue architectures. Figure 4a shows an epithelial cell-lined 3D branching ductal geometry with open lumens, designed to mimic natural epithelial forms (see Extended Data Fig. 11a, 11b). Next, we focused on a general design motif pervasive in many natural tissues where independent networks weave through each other in proximity but never come in direct contact. Specifically inspired by the coordinated architecture of the lymphatic and blood vessel networks[39], we designed dead-ended branching lymphatic channels woven into a perfused, branching blood network (see Fig. 4b). To align the two distinct networks, we incorporated support structures into the design that registered these Ga pieces at the extreme ends outside the gel region (Extended Data Fig. 11c, 11d; see Methods). Following ESCAPE and seeding the separate regions with blood and lymphatic ECs, confluent enmeshed dual 3D networks are formed (see Fig. 4c–4d, Extended Data Fig. 11e–11g, & Supplementary Video 13). Next, to demonstrate ESCAPE's potential in organizing a metabolically demanding tissue, we designed twisted pairs of 3D muscle bundles nourished by nearby vascular conduits (see Fig. 4f & Extended Data Fig. 12a–12b). We first studied the contractile functionality of the cardiac bundles (maximally packed with 90% iPSC-CMs and 10% CFs; see Methods) alone without the endothelial cells in the vascular conduits (Extended Data Fig. 12c–12d). Upon electrical stimulation, the cardiac bundles contracted, straining the surrounding matrix and affecting the overall flow profiles in the nearby vascular conduit visualized by the flow of beads (see Extended Data Fig. 12e–12g & Supplementary Video 14–15). Upon subsequent endothelialization of the vascular conduit (Fig. 4f–4g, Extended Data Fig. 12h,12i), cell-dense 3D cardiac bundles with integrated vasculature are generated that feature contractile function (Fig. 4h, Supplementary Video 16)—paving way for future tissue engineered constructs with built-in vasculature.

Summary and conclusion

Biological function is closely tied to multiscalar forms that have largely remained challenging to engineer in natural materials. Here we present a powerful new means to fabricate multiscalar shapes using gallium ESCAPE molding. To aid the design process we developed basic guidelines to form casts and extract them through capillary forces; in the future, simulating gallium ESCAPE will enable one to include efficient capillary withdrawal as a design metric. Whereas much of the focus here was on multiscalar vascular forms—to highlight the capabilities of the ESCAPE process—the ability to now achieve both microscale control of geometry as well as build hierarchical constructs opens new opportunities in the generation of an expansive set of organotypic designs and tissue architectures.

Methods

Materials.

Polydimethylsiloxane (PDMS) was prepared by mixing Sylgard 184 base with the curing agent at 10:1 ratio (SYLGARD™ 184 Silicone Elastomer Kit, Dow Inc., MI, USA), degassed and cured in an oven at 60 °C for 2+ h (typically overnight). Gallium was used as purchased (50 g tubes, CAS 7440-55-3 Luciteria Science, WA, USA). Solutions of NaOH were prepared by serial dilution from a 5N solution (Sodium Hydroxide 5N, #SS256–500, Thermo Fisher Scientific, MA, USA) with ultrapure water (Milli-Q, Direct-Q UV Remote Water Purification System, MilliporeSigma). Collagen gels (2.5 or 4 mg/ml) were prepared from high concentration 8–11 mg/ml rat tail collagen I stocks (#354249, Collagen Type I, high concentration, rat tail, Corning Inc., NY, USA) based on a general protocol for forming 3D collagen gels[40]. Briefly, collagen was buffered with a 10× reconstitution buffer (10× RB is made of 2.2 g sodium bicarbonate and 4.8 g HEPES in 100 ml distilled water) and 10× DMEM (#D2429, Sigma-Aldrich), titrated to a pH of 9 with 1M NaOH and diluted with phosphate-buffered saline (PBS) to a final concentration (2.5 or 4 mg/ml), all in an ice bucket. This pre-gel solution was injected into chambers as desired and left to polymerize overnight at room temperature (RT) in a humid atmosphere to prevent evaporation. Fibrin gels were formed by first dissolving fibrinogen from bovine plasma (#F8630, Sigma-Aldrich) at a concentration of 5mg/ml in DPBS (#14287080, Thermo Fisher Scientific) at 37 °C and sterile filtering (0.2 μm filter). The fibrinogen solution was mixed with thrombin (#T4648, Sigma-Aldrich) at a ratio of 0.1U of thrombin per mg of fibrinogen and immediately injected into desired regions and left to clot. Agarose gels were formed by dissolving 5% w/v of ultra-low gelling temperature agarose (#A5030, Sigma-Alrich) in PBS at 60 °C. Prior to injection the devices were cooled (optional) and agarose was injected into the devices as the solution was cooling.

Cell culture.

Human microvascular blood endothelial cells (dermal hMVECs; #CC-2813, Lonza, Switzerland) were cultured and maintained in Microvascular Endothelial Cell Growth Medium-2 (EGM2-MV media: EBM-2 basal media (Lonza) supplemented with the MV2 bullet kit). Human umbilical vein endothelial cells (hUVECs; #C2519A, Lonza) were cultured and maintained in EGM-2 media (Lonza). hMVECs and hUVECs were used at passages 4–6. LifeAct-Ruby-hUVECs (mRuby-hUVECs) were generated and described in a previous study[41] and cultured in EGM-2 media. Human epithelial cells (colorectal adenocarcinoma cells, Caco-2; ATCC) were cultured and maintained in a medium containing DMEM/F-12 (#11320033, Thermo Fisher Scientific) supplemented with 10% FBS (#F0926, Fetal Bovine Serum, Sigma-Aldrich) and 1% v/v penicillin-streptomycin (Invitrogen). Dermal lymphatic endothelial cells (Pooled human dermal microvascular endothelial cells; mixed population of blood and lymphatic ECs, #CC-2516, Lonza) was used as the source of lymphatic ECs. Lymphatic ECs (Prox1-positive) were cultured and maintained in EGM2-MV and were used at passages 4–6. Human ventricular cardiac fibroblasts (CFs; #CC-2904, Lonza) were cultured and maintained in Cardiac Fibroblast Growth Media (FGM-3; #CC-4526, Lonza) and used at passages 4–7. Human induced pluripotent stem cell-derived cardiomyocytes (iPSC-CMs) were differentiated from an

iPSC line (PGP1 parent line subclone with green fluorescent protein (GFP) tagged to endogenous titin (TTN)) manipulating the Wnt signaling pathway using previously reported methods[42,43]. Briefly, iPSCs under monolayer culture (RPMI medium with B27 minus insulin; Thermo Fisher Scientific) were first Wnt-activated using 12 μM CHIR99021 (#4423; Tocris Bio-Techne Corporation, MN, USA) on day 0 for 24 h and then Wnt-inhibited using 5 μM IWP4 (#5214; Tocris Bio-Techne) on day 3 for 48 h. On day 9, cells were switched to culture in RPMI medium with B27 with insulin (Thermo Fisher Scientific) and underwent metabolic selection on day 11 in 4 mM sodium DL-lactate in glucose-free RPMI (Thermo Fisher Scientific) for 4 days. After metabolic selection, iPSC-CMs were replated onto fibronectin-coated 12-well plates (10 μg/ml fibronectin; #356009; Fisher Scientific) and maintained in RPMI supplemented with B27 with insulin for at least 2 weeks (day 30+) prior to using in experiments. All cells were maintained at 37 °C in 5% CO_2 in humidified incubators.

Antibodies and reagents.

Anti-VE-cadherin (F-8, 1:500 dilution) was from Santa Cruz (#sc-9989, Santa Cruz, TX, USA). Anti-VE-cadherin (D87F2, 1:500 dilution, #2500S) and Anti-E-cadherin (24E10, 1:1600 dilution, #3195S) were from Cell Signaling (Cell Signaling Technologies, MA, USA). Phalloidin conjugated with Alexa Fluor 488 (#A12379), phalloidin conjugated with Alexa Fluor Plus 555 (#A30106), phalloidin conjugated with Alexa Fluor Plus 647 (#A30107) were purchased from Invitrogen/Thermo Fisher and prepared as a DMSO stock solution (~66 μM) and used at 1:1000 dilution. Anti-Prox1 (#102-PA32, 1:500 dilution of 0.5 mg/ml stock) primary was from ReliaTech (ReliaTech GmbH, Wolfenbüttel, Germany). Ulex Europaeus Agglutinin (UEA Lectin) DyLight 649 (1:250 dilution) was from Vector Labs (#DL-1068–1; Vector Labs, CA, USA). Anti-mouse and anti-rabbit secondary antibodies with Alexa Fluor Plus 488, 555 and 647 (#A32790, #A32773, #A32733), and DAPI (#D3571) were from Invitrogen/Thermo Fisher and used at 1:1000 dilution. LIVE/DEAD viability/cytotoxicity kit for mammalian cells was purchased from Invitrogen/Thermo Fisher (#L3224) and used following the manufacturer recommended protocol.

Ga adhesion experiments.

12 mm wide holes were punched out of ~0.25” thick slabs of PDMS. PDMS pieces and glass coverslips were then plasma cleaned at 100 W for 30 s (EMS Quorum 1050x, EMS, PA, USA) and bonded together to form wells. For PDMS-Ga adhesion experiments, the internal surfaces of the wells were coated with freshly mixed 10:1 PDMS (monomer: crosslinker) and cured at 100 °C for at least 1 h. For PDMS-agarose adhesion experiments, a layer of freshly prepared 5% w/v of ultra-low gelling temperature agarose (#A5030, Sigma-Alrich) in PBS was added to the bottom of the wells, sealed with tape to prevent evaporation and gelled at 4 °C for 1h. Beads of liq. Ga (~3 mm) were added to wells with freshly prepared PDMS or agarose gels respectively and left overnight to form an oxide layer and stabilize their interface with the underlying substrate. When low concentrations of NaOH (10 mM) was added to stabilized liq. Ga droplets on agarose substrates, the Ga droplets quickly formed spheres and were easily dislodged (< 10 s) upon tilting. However, with 10 mM NaOH exposure, Ga droplets on PDMS substrates lost the oxide layer and turned shiny

in the same period (as previously described[44]) but remained adhered (Supplementary Fig. 1 & Supplementary Video 1). To quantify the adhesion between Ga and PDMS, these wells with stable liq. Ga drops were filled with different concentrations of NaOH, covered with a glass coverslip and flipped. When the oxide layer was fully removed and the hanging droplets of liq. Ga detached from the PDMS, they formed spheres and dropped down (see Supplementary Video 1); the time to detach is quantified in Supplementary Fig. 1b. Overall, Ga adheres to PDMS much more strongly than water-based gels and requires high concentrations of NaOH (~1 M) to detach from PDMS in minutes.

Ga filament fabrication.

150 μm-diameter cylinders were designed in a computer aided design (CAD) software (SolidWorks, Dassault Systèmes SE, France) and printed on pre-treated silicon substrates. To prepare silicon substrates for printing, they were plasma cleaned at 100 W for 30 s (EMS Quorum 1050x, EMS, PA, USA) and left overnight in a vacuum desiccator with 20 μL of 3-(trimethoxysilyl) propyl acrylate (#475149 Sigma-Aldrich, MilliporeSigma, MA, USA). The design was printed on the treated silicon substrate using a commercial two-photon direct laser writing system (Photonic Professional GT, Nanoscribe GmbH, Germany) with a 25× objective with the photoresist IP-Dip (Nanoscribe GmbH). The printed parts were cleaned in polyethyl glycol mono ether acetate (PGMEA, #484431 Sigma-Aldrich) for 30 min to remove uncured resist and rinsed with isopropanol (IPA) followed by Novec™ 7100 (3M Company, MN, USA) and left to dry for 2+ h. To make the printed mold non-adhesive in subsequent steps, the part was plasma cleaned for 100 W at 30 s and silanized for 3 h in a vacuum desiccator with trichloro(1H,1H,2H,2H-perfluorooctyl)silane (#448931, Sigma-Aldrich). The negative copy of the shape was formed by polymerizing PDMS around the structure. Gallium was melted at 45 °C and injected into the cylindrical void after which it was solidified and extracted from within the PDMS to form a freestanding Ga filament.

Ga filament evacuation.

To first test the ESCAPE process with linear Ga filaments, the filaments were assembled into a PDMS device consisting of a 6-mm wide chamber (Fig. 1a). The PDMS devices with chambers were fabricated from negative molds (designed in SolidWorks) and printed commercially (Protolabs, MN, USA). PDMS chambers and glass coverslips were plasma cleaned at 100 W for 30 s and let to cool briefly after which they were bonded together after placing the Ga filaments to span the chamber. The devices were left to sit overnight in RT and were cleaned with ethanol. To prepare the internal surface of the PDMS chambers for gel attachment, the assembled chambers were treated with a 0.5 mg/ml solution of dopamine hydrochloride in tris buffered saline (diluted from 10× Tris Buffered Saline, #T5912, Sigma-Aldrich, and adjusted to a pH of 8.5 with a 5 N NaOH solution) for 1 h. After this, the devices were rinsed in DI water, followed by 50% ethanol (in DI water) and ethanol and left to dry in a vacuum chamber for 2 h. Alternatively, the chambers could be treated with poly-L-lysine (PLL) followed by glutaraldehyde to promote collagen binding as described previously[33]. After surface treatment and drying, 2.5 mg/ml collagen pre-gel solution was prepared as described in the section ‘Materials’ and injected into the gel chambers and left to polymerize overnight at RT in a humid environment. Next day, until gallium evacuation, to prevent any evaporation of water from the gel, PBS was added to the reservoirs at both ends

of the chambers. To begin evacuation, devices were placed on hotplate (Benchmark) set to 32 °C; the melting of Ga filaments can be observed typically within 2–5 min. Then the extra PBS previously added to the end reservoirs were removed and replaced with NaOH solution of the desired concentration; the right reservoirs were filled with more liquid to create a pressure head for NaOH solution to reach into the evacuating end. Images were captured every 2 s (Canon EOS 6D Mark II with macro lens Canon EF 180mm f/3.5L Macro USM) and made into a timelapse at 30 Hz. For the 10 mM NaOH condition in Fig. 1b, fresh 10 mM NaOH solution was added once at the 11 min mark to reestablish the pressure head.

Second harmonic generation (SHG) characterization of collagen.

To study the dimensional stability of collagen cavities upon exposure to NaOH solutions, needle molded collagen gels were formed first. 4 mg/ml collagen gels (as described in the section 'Materials') were polymerized in surface-treated PDMS chambers (see 'Ga filament extraction' section for treatment procedure) around 160μm sized needles (that were pre-soaked in 0.1% bovine serum albumin solution for 1 h; prepared from #A2058, Bovine Serum Albumin, Sigma-Aldrich). Following overnight gelling, the needles were removed leaving cylindrical conduits of 160 μm diameter (Extended Data Fig. 1a). The two reservoirs connecting the cylindrical channel were filled with a total volume of 75 μl of either PBS (control), 10 mM, 20 mM, 50 mM, or 100 mM NaOH solutions with a pressure head to cause flow through the channel and placed on a hot plate at 32 °C for 30 min. Following this, the devices were removed and rinsed in PBS 3 times. Collagen architecture was analyzed through SHG images that were obtained with a Leica TCS SP8 MP multiphoton microscope equipped with a tunable (680–1300 nm) fs laser (InSight DeepSee; Spectra-Physics, CA, USA) set to 885 nm excitation. Second harmonic generation signal was recorded with the HyD-RLD 2-channel detector (non-descanned detection) with the SHG 440 filter cube (BP 440/20 nm and BP 483/32 nm filters) using the HC FLUOTAR L 25×/0.95 and HC APO L U-V-I 10×/0.3 water immersion objectives. The dimensions of the vessel were measured using ImageJ; first, the central slice of the volumetric stack was identified, and the lumen size was measured from the central slice. For bulk collagen intensity measurement (Extended Data Fig. 1d), 5mm wide circular wells were punched out of ~1 mm thick PDMS sheets that were then bonded to a glass cover slip. 25 μl of 4 mg/ml collagen was added to each well and polymerized overnight as described previously, forming ~1 mm thick collagen gels. These gels were submerged in different concentrations of NaOH for 30 min at 32 °C after which they were rinsed in PBS and imaged. Averaged intensity profiles in Extended Data Fig. 1b and bulk average collagen SHG intensity in Extended Data Fig. 1d were computed using MATLAB (MathWorks, MA, USA).

General ESCAPE process.

First, the intended geometry was designed using constructive solid geometry using interactive CAD tools (SolidWorks) or procedural CAD modelers like OpenSCAD (http://openscad.org/) and Blender 2.91 (Blender Foundation). The geometries were designed based on the design criteria described in Supplementary Information. A version of the original Stanford Bunny model (URL: http://graphics.stanford.edu/data/3Dscanrep/#bunny) was downloaded from the URL: https://github.com/dcoeurjo/VolGallery/tree/master/Stanford-bunny and used for Fig. 1d–1e and Extended Data Fig. 2. For generating the initial mold in

this work, a two-photon direct laser writing system (Photonic Professional GT, Nanoscribe GmbH) was used with a 25× objective with the photoresists IP-Dip and IP-S (Nanoscribe GmbH). Following the approach in section 'Ga filament fabrication', the printed molds were cleaned, surface treated with trichloro(1H,1H,2H,2H-perfluorooctyl)silane, and PDMS was crosslinked around the mold to make the negative structure. For most designs, a PDMS monomer to crosslinker ratio of 10:1 was used (except for some 3D designs like the Stanford Bunny design and 3D branching vascular network design where 20:1 ratio was used to make a softer PDMS). The gallium cast was formed by placing molten gallium on top of a cavity, forming a sealed enclosure, and applying and releasing vacuum. In designs with small features, upon releasing vacuum, the PDMS negative with infilled gallium was placed on a hot plate and additional pressure was applied manually for liquid gallium to reach the smallest regions (see Supplementary Information and Supplementary Fig. 3 for a discussion of the criteria). The excess gallium was then removed with a wipe soaked in ethanol and the PDMS negative with infilled gallium was cooled to 4 °C after which the supercooled liq. Ga was brought into contact with a crystalline structure to initiate solidification. The solid gallium cast was typically separated from the PDMS negative by peeling the PDMS after solidifying the Ga cast. In designs like the overhand knot (Fig. 2d), 3D hierarchical tree (Fig. 3f), orthogonal networks (Fig. 4b) and cardiac bundles (Fig. 4e) where the PDMS negative cannot be removed without deforming the solid Ga cast, the PDMS negative was etched using a selective etch. A 1:4 ratio of 1M tetrabutylammonium fluoride (TBAF) in tetrahydrofuran (#216143, Sigma-Aldrich) to acetone was used to etch PDMS; acetone was used as a solvent due to its low swelling index and that the combination of TBAF and acetone yielded a high etch rate[45]. The duration of the etch was typically under an hour and was timed based on the size of PDMS to be etched. The Ga cast was rinsed in ethanol and then left to dry. Typically, Ga casts were assembled into PDMS devices with chambers to hold the soft gel. PDMS chambers and glass coverslips (24 mm × 30 mm, No. 1, #48393–092, VWR, PA, USA) were cleaned in a plasma asher (EMS Quorum 1050x, EMS, PA, USA) for 30s at 100W and left to cool for 1–2 min. The PDMS devices were bonded to the glass coverslips with the Ga cast inside and left to bond overnight. The assembled chambers were treated with 0.5 mg/ml dopamine hydrochloride in tris buffered saline for 1 h, rinsed in DI water, followed by 50% ethanol and ethanol, and left to dry in a vacuum desiccator for 2 h as described in section 'Ga filament evacuation'. After this, the soft gel material of choice (agarose, collagen or fibrin) was injected into the gel chambers around the Ga cast and left to gel following the description in the section 'Materials'. PBS was added to the devices to prevent evaporation of the hydrogels post gelling. To evacuate the Ga cast, the PDMS devices were placed on a hot plate at 32 °C to first melt the Ga cast. The process was monitored continuously using a stereo microscope (ZEISS SteREO Discovery V20 Motorized Stereo Microscope, Carl Zeiss, Germany). Typically, 10 mM NaOH was used to remove the surface oxide of gallium (unless noted otherwise); a fluidic pressure head was created from the retracting end to the collecting end to ensure that NaOH solution reached all parts of the devices through the bulk interstitial space to remove the surface oxide of gallium. The pressure head was restored (approx. every 10–15 min) with fresh NaOH solution to ensure flow through the gel interstitial space. After complete gallium evacuation, the gallium droplets collected in the reservoirs were removed, and the gels and reservoirs were washed with PBS 3 times. After inspecting the devices in the stereo microscope, fresh

PBS was added to the reservoirs with a pressure head to ensure flow through the cavities and the gels, after which the devices (soaked in PBS) were stored at 4 °C overnight. At this stage all NaOH is considered to be fully washed out from the gel; measured pH is same as that of PBS.

General device seeding and culture.

The PDMS devices with the soft gels after gallium evacuation through ESCAPE were stored with PBS in the reservoirs at 4 °C. The night prior to cell seeding, the devices were brought to room temperature and the PBS was removed from the reservoirs and the gel regions. 50 μl of fresh cell culture media depending on the intended cell type (e.g., EGM-2MV for hMVECs) was added to each media reservoir. The devices were then transferred to a rocker inside a tissue culture incubator (humidified; 37 °C with 5% CO_2) for at least 4 h (typically overnight). On the day of cell seeding, cells were lifted from cell culture dishes with 0.05% trypsin/EDTA (Gibco) and centrifuged at 200 g for 4 min. Cells were then resuspended in the growth medium at a density of 1×10^6 cells/ml (counted with a hemocytometer). In total 50–70 μl of cell suspension was added across the two reservoirs for the cells to flow into the gel conduits; devices were occasionally flipped and turned for cells to reach different parts of the conduits (over the course of ~5 min) after which the devices were store in the incubator for 15–30 mins for the cells to attach. Following this, the excess cell solution was removed from the reservoirs and 50 μl of cell culture media was added to each reservoir and the devices were placed on a rocker in the incubator. Culture medium was changed daily, and the devices were observed through a brightfield microscope for cell confluence; typically, full confluence was achieved 2–3 days after seeding.

Immunofluorescence and microscopy.

Devices containing cell-lined vessels and cavities were fixed with a 4% paraformaldehyde (Electron Microcopy Sciences) in PBS for 15–30 min. Devices were then washed with PBS and permeabilized with 0.15% Triton X-100 (Sigma-Aldrich) for 15–30 min at RT in the presence of a pressure head to ensure that solution reached all areas of the device. The devices were then blocked with 3% BSA for 1h at RT (or overnight at 4 °C). The devices were then washed in PBS thrice and primary antibodies and phalloidin in 3% BSA (at the respective dilutions stated in section ‘Antibodies and reagents’) were added to the device and left overnight at 4 °C. Next, the devices were washed 2 times in PBS and fresh PBS was added to the device ports and left at 4 °C in the presence of a fluidic pressure head for 2 h. The solution was then replaced with the secondary antibodies in 3% BSA and stained overnight at 4 °C. Next day, the devices were washed thrice in PBS and cell nuclei were marked with DAPI for 1 h after which the devices were washed in PBS. Immunofluorescence images of the devices were obtained using a Leica TCS SP8 MP multiphoton microscope with the HC FLUOTAR L 25×/0.95 and HC APO L U-V-I 10×/0.3 water immersion objectives. Tile scans were controlled and obtained at constant laser intensity using the LAS-X software (Leica). Images were adjusted uniformly for contrast and brightness using ImageJ. ImageJ was also used to generate composite images, z-projections, depth-coded images, and stitch tile scans. 3D volumetric views of the vascular malformation (Extended Data Fig. 6d) were generated with Imaris 9.7.2 (Oxford Instruments, UK). Brightfield images (Extended Data Fig. 2b, 2d, 5e, 6b) were acquired

using a Nikon Eclipse TE200 microscope. Scanning electron microscope (SEM) images were acquired with a Field Emission Scanning Electron Microscope Zeiss Supra 55VP (Carl Zeiss, Germany); prior to SEM imaging samples were optionally surface coated with Au/Pd using a Cressington 108 sputter coater (Cressington, UK).

Comparing ESCAPE in porous hydrogels v. non-porous materials.

To compare the effectiveness of the ESCAPE process in conduits in hydrogels and non-porous materials, we used the design of a vessel that branches into two daughter vessels, one of which is dead ended (Extended Data Fig. 3a; bottom). Ga casts were formed as previously described and assembled into PDMS devices with chambers to hold the gels. 5% agarose was used as the porous gel and PDMS was used as the non-porous material Gallium evacuation was performed with 10 mM NaOH in the agarose gel. Since gallium adheres to PDMS more than water-based gels, and with PDMS being more hydrophobic, a high concentration of NaOH (100 mM) was used for switching the surface tension of gallium.

Live-dead assay.

The effects of culturing cells in direct contact with gallium were evaluated by adding ~5 mm sized droplets of gallium onto the center of the wells in a 6-well plate. Culture media was added and pre-warmed in these wells following which hMVECs and hUVECs were seeded at low confluence (~20%) and cultured for 4 days. Cell culture medium was changed once 2 days after cell seeding. The live/dead assay was performed using the cell viability kit (see 'Antibodies and reagents' section) following the recommended protocol and imaged from the top using the Leica TCS SP8 MP multiphoton microscope.

Characterization of Ga remnants—Energy dispersion spectroscopy (EDS) analysis and particle counting.

A mold geometry with 4 vertical posts (see Supplementary Fig 4a) was used to generate collagen structures (4 mg/ml) using the full ESCAPE process. The solvent in these hydrated collagen samples was gradually switched out from PBS to ethanol (through soaking in 25%, 50%, 70%, 80%, 90% ethanol intermediates for 30 mins each). Finally, the samples were left overnight in pure ethanol, and then critical point drying (CPD) was performed (SAMDRI manual critical point dryer, tousimis, MD, USA). Collagen surfaces in direct contact with Ga prior to Ga evacuation were inspected post-ESCAPE for Ga residues through EDS analysis (Phenom PROX Desktop SEM with EDS; Thermo Fisher Scientific, MA, USA) with an accelerating voltage ≥ 10 kV. Elemental maps showed spherical residues to Ga (Supplementary Fig. 4b) on exposed collagen surfaces corresponding to 0.18% (atomic conc) through regional analysis (Supplementary Fig. 4c). To account for environmental contaminants that potentially underreport the amount of Ga, spot analysis was performed on Ga residues (that ideally must report 100% Ga). These spots reported 69.8% (atomic conc.) Ga; the remaining fraction is considered as contaminants (Supplementary Fig. 4d–4e). Second, to calibrate for noise in measurements that potentially result in overreporting the amount of Ga, spot analysis was performed on collagen surfaces that never were in contact with Ga and found 0.10% (atomic conc.) of Ga. Using these two calibrations, the adjusted Ga residue is 0.11% (atomic conc.). In summary, the total Ga residues are measured as 0.11% (atomic conc.; corrected) or 0.18% (atomic conc.; uncorrected) as measured

through EDS. Next, 13 samples were analyzed through SEM imaging and particle counting (ImageJ). The microscale particulates covered 0.2% of the total imaged area (Supplementary Fig. 4f).

Diffusive permeability measurement.

Linear vessels (150 μm diameter) were fabricated using the general ESCAPE process in 4 mg/ml collagen. For the cell-lined vessel group, hMVECs were seeded into the channels and cultured for 3 days until a confluent monolayer was formed. A group of empty vessels (i.e., without endothelial cells) was prepared simultaneously as control. Both groups of devices were cultured on a rocker inside a tissue culture incubator (humidified; 37 °C with 5% CO_2) prior to the vascular barrier measurement. To assess the vascular barrier function of ESCAPE fabricated vessels, a previously reported protocol to measure diffusive permeability was used[33]. Briefly, devices were removed from the rocker and brought to an environment controlled confocal microscope (humidified; 37 °C with 5% CO_2). The vessel was aligned in brightfield such that the entire width of the vessel was visible near the bottom of the imaging area and a large portion of the bulk gel on one side was visible on top. Focus was adjusted to the widest region of the vessel and 50 μL of 70-kDa fluorescent dextran (Dextran, Texas Red™, #D1830, Thermo Fischer Scientific) diluted to 12.5 μg/ml in PBS was added to one of the media ports. Fluorescent dextran flowing through the vessel and diffusing into the gel region were imaged in each frame (150 frames; 5s interval between frames; see Supplementary Video 10). The vessel was manually segmented for each device to then define the vessel and bulk gel area in MATLAB. The diffusive permeability coefficient was then calculated as $P_D = \left(2r/I_0\right)\frac{dI}{dt}$ where r is the radius of the vessel, I_0 is the fluorescent intensity in the vessel region, and I is the fluorescent intensity in the bulk gel region (Supplementary Fig. 6). Compared to empty collagen vessels (i.e. with no cell-lining; control) with mean $P_D = 51.6 \times 10^{-6}$ cm/s, cell-lined vessels had significantly reduced diffusive permeability $P_D = 12.2 \times 10^{-6}$ cm/s (or stronger vascular barrier) as measured across 15 devices per condition.

Quantifying actin alignment.

From the volumetric images of the vessels, the central slice was identified in ImageJ and the maximum z-projection of one half of the vessel was obtained. Maximum z-projection of the entire vessel was used when a single image slice did not separate the entire imaged region into two clear halves. The following automated approach was used to quantify the overall alignment of actin filaments in the vessels with the topographical cues (Fig. 2f, Extended Data Fig. 6e–6g and Supplementary Fig. 7). The F-actin channel of the maximum z-projection images were loaded in MATLAB and a 20 μm long structuring element (angle iteratively varied from 0° to 360° in 1° increments) was used to perform a morphological opening of the image. From the central part of the vessel, the pixels in the actin image with a high degree of alignment were automatically estimated from the morphological opening intensities. The peak alignment direction was recorded from these regions and a polar histogram was generated to highlight the orientation of the actin bundles.

Deterministic branching vascular tree designs.

The branching tree with 5 hierarchical levels with 2 dead-ended branches and 1 through branch at each level (Fig. 3a) was designed procedurally in OpenSCAD such that $\sum r^n$ is conserved where the exponent n = 3 in ideal Murray's law. For the design in Fig. 3a, an exponent of $n = 2.96$ was used to demonstrate that n can be varied in design easily. The fully perfusable branching tree design in Extended Data Fig. 7e with 1 inlet and 32 outlets, and the 3D branching tree (Fig. 3f) with 1 inlet and a 4 × 4 array of outlets were generated using the Blender Python API (Blender Foundation). The vessel calibers were based on the ideal Murray's law exponent $n = 3$.

Design of space colonization trees.

Computationally designed vascular trees were generated based on our custom implementation of the space colonization algorithm[37,38] in Blender with the Python API. Briefly, a set of N virtual cells (or attractors) were randomly distributed within a specific boundary. For results in Extended Data Fig. 8, the boundary was defined to be a 4 mm × 4 mm square region. The starting node of the tree was defined to be near (or inside) this boundary. The tree is grown iteratively such that all the cells are 'nourished', i.e., within a predefined vessel-cell distance (VCD) from the branches of the vascular tree; this is analogous to living cells being within a diffusion length away from blood vessels in natural tissues. In each iteration, virtual cells that are within a predefined distance-of-influence (DOI) but not nourished by the vascular tree (i.e., not within VCD from any of the branches of the tree) attract the node closest to them. Cells outside the DOI are treated to be too far to influence the tree growth. New segments of the tree are added from all the nodes attracted by cells towards the average direction of all cells attracting that specific node (the growth vector); random noise and tortuosity factor (TF) are optionally added to the growth vector in this step of the algorithm to make the vessel segments tortuous. Step size is the spacing between the nodes during the tree growth. This process is continued until all the cells are within distance VCD from the tree (or a maximum number of iterations is reached) and yields a tree skeleton. The generated tree skeleton is automatically cleaned to remove single segment branches. After cleanup, the tree skeleton is sized according to natural scaling laws law starting with the terminal branches of the tree, e.g., in Extended Data Fig. 8, the terminal branches are designed to have a radius of 25 μm and all parent vessels are sized such that $\sum r^3$ is conserved. The vascular tree fabricated using ESCAPE (Fig. 3c, 3d and Extended Data Fig. 9) was generated with the following parameters: 4 mm × 4 mm boundary, N = 1000 cells, DOI = 1000 μm, VCD = 100 μm, step size = 50 μm, radius of terminal vessels = 25 μm; Supplementary Video 11 shows the growth of the tree through the different iterations.

In the above examples, the overall boundary was fixed throughout the iterations. To simulate organ growth, the boundary of the vascular tree can be expanded each iteration as desired, at a defined growth rate (called marginal growth). The marginal growth tree design in Extended Data Fig. 10a and Fig. 3e was generated using the sector of a circle (with sector angle 53.1°) as the boundary but whose radius was grown at a rate of 12.5 μm each iteration up to a maximum radius of 4 mm. Virtual cells were added at a uniform areal density as the boundary was expanded. The marginal growth tree was generated with the following

parameters: total $N = 10000$ cells, DOI = 1000 μm, VCD = 150 μm, radius growth rate = 12.5 μm/iteration, step size = 50 μm, and radius of terminal vessels = 25 μm.

Gallium evacuation rates during ESCAPE in large vascular trees.

Space colonization vascular trees were fabricated as described in the section 'General ESCAPE process'. In large vascular tree designs, during the evacuation of gallium with the ESCAPE process, liquid gallium flowing out from all the terminal branches is collected through one central root vessel, e.g., in the designs in Fig. 3d. To investigate whether the gallium evacuation during the ESCAPE process was limited by the flow rates through this central vessel, the evacuation of this tree was compared when 20 mM NaOH and 100 mM NaOH solutions were used (Extended Data Fig. 9c, 9d). When exposed to high concentrations of NaOH, the surface oxide at all branches is removed causing all the terminal branches to evacuate at once as opposed to a more directional evacuation at lower concentration. This experiment shows that liquid gallium evacuation is not limited by the flow rate of liquid exiting through the parent vessel but by how many terminal branches are actively pumped out simultaneously (Supplementary Video 12).

3D applications of ESCAPE—vascular networks, orthogonal networks and cardiac bundles.

In 3D architectures like the overhand knot (Fig. 2d), 3D hierarchical tree (Fig. 3f), orthogonal networks (Fig. 4b) and cardiac bundles (Fig. 4e) narrow walls were projected onto the substrate to make the designs moldable to generate the PDMS negative (see Extended Data Fig. 5, 10, 11 and 12). In general, the supporting walls are made to be thinner than the smallest feature of the design such that a pressure threshold can be found so that Ga can be selectively injected into the desired portions of the PDMS negative and not the thin walls. In these designs, upon solidification of the Ga cast, the PDMS negative is selectively etched to release the Ga cast as described in the section 'General ESCAPE process'. In the overhand knot and 3D hierarchical tree examples, ECs are seeded into the channels, cultured under flow and imaged as described previously.

In the orthogonal network design, the Ga cast includes the interwoven lymphatic and blood networks and an additional Ga supporting structure to register the pieces together (Extended Data Fig. 11c, 11d). In this device, an external PDMS structure ensures that the collagen gel is added only in the central portion of the structure featuring the two networks, i.e., the supporting arc is designed to fall outside the gel region. The port connected to the lymphatic inlet, and the two ports connected to extreme ends of the blood network are isolated from each other using agarose (5% w/v of ultra-low gelling temperature agarose; #A5030, Sigma-Alrich) as a sealant. This scheme allows one to generate complete distinct and orthogonal cavities with ESCAPE. For cell seeding, the lymphatic ECs were first lifted from culture dishes (suspension density ~ 1×10^6 cells/ml) and seeded into the dead-ended lymphatic network as described in the 'General device seeding and culture' section. These devices were transferred to the incubator (static culture) for 4 h for the lymphatic ECs to attach to the collagen gel. Blood endothelial cells (hMVECs) were subsequently lifted from culture dishes, brought into suspension (density ~ 1×10^6 cells/ml) and seeded into

the blood network. These devices were returned to the incubator and cultured on a rocker oriented such that flow is directed along the blood network.

The cardiac bundle design incorporates two noteworthy features (Extended Data Fig. 12a, 12b): first, alignment tabs are used at the extreme ends of the device to register the Ga pieces corresponding to the cardiac regions and the nearby vascular conduit. Second, the tubes gradually taper at the ends down to 70 μm diameter (shown on the right) so that cardiac cells can be intentionally brought to clog at the right ends to maximally pack cardiac cells. The Ga cast was evacuated as per the general ESCAPE process; here again, the alignment tabs fall outside the gel region. The cardiac regions of these devices were first seeded with a cell suspension containing a mixture of iPSC-CMs (90%) and CFs (10%) at a combined cell density of 2.22×10^6 cells/ml. At this cell density, the cells clog at the tapered ends and backfill to form maximal packing densities throughout the cardiac bundle region (Extended Data Fig. 12c). These cardiac-only devices were cultured in media containing high glucose DMEM (Fisher Scientific) supplemented with 10% fetal bovine serum (FBS; Millipore Sigma), 1% penicillin-streptomycin, 1% non-essential Amino Acids (Fisher Scientific), 1% Glutamax (Fisher Scientific), 5 μM Y-27632 (#1254; Tocris Bio-Techne) and 0.033 mg/ml aprotinin (Millipore Sigma). Aprotinin and Y-27632 were removed from culture media after 1 day, and media was replaced daily. To generate devices with both cardiac bundles and endothelial cell-lined vasculature, cardiac cells were seeded first as described above. After 1 day of culture, the media was changed to EGM2-MV and the devices were placed on the rocker for at least 4 h to prepare the vascular conduits for EC seeding. mRuby hUVECs were seeded on to the vascular conduits at a cell suspension of 1×10^6 cells/ml. The smaller size and the lower cell suspension density prevented the ECs from clogging (unlike the iPSC-CMs in the cardiac portions) and getting packed throughout the vascular conduits. These devices were returned to the rocker with EGM2-MV as the maintenance media for two additional days for the ECs to form a confluent monolayer. Live imaging was performed for both sets of devices using 4× and 10× objectives on a Nikon Eclipse Ti microscope (Nikon Corporation, Tokyo, Japan) in an environment-controlled chamber (humidified; 37 °C with 5% CO_2). Devices were electrically stimulated using 20V waveforms (Extended Data Fig. 12e) generated with an IonOptix C-Pace EP cell culture stimulator (IonOptix LLC, MA, USA) and delivered using platinum wires (#EP1330; Sigma-Aldrich CVS10 replacement platinum wire; Millipore sigma) immersed in the two furthest media reservoirs. Cardiac contractions were recorded at a frame rate of 30Hz (Supporting Video 14). To study the effect of cardiac contractions on the flow through the vascular conduit, 5 μl of beads were added at 1:1000 dilution (Polybead Dyed Microsphere Kit – 1 μm; #16906–1, Polysciences, PA, USA) to one of the vascular media reservoirs to create a small pressure head. Kymographs (position-time maps) were generated along specific paths in the acquired videos (30 Hz frame rate) with ImageJ to map the flow of tracer beads (Extended Data Fig. 12g & Fig. 4h).

Extended Data

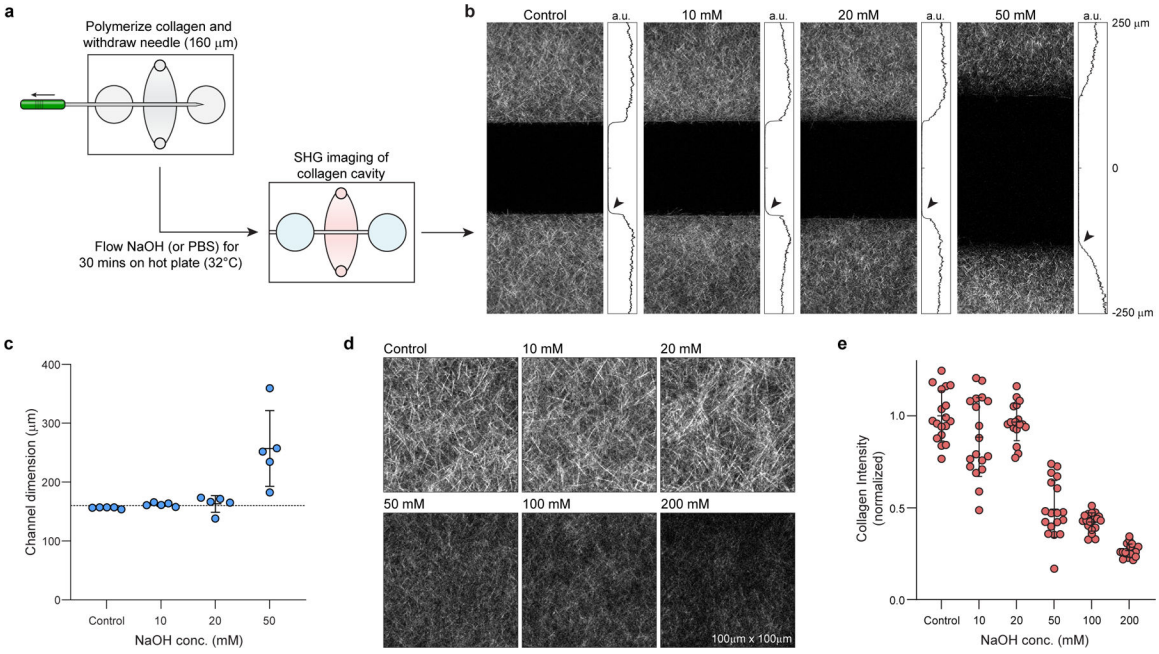

Extended Data Fig. 1 |. Characterization of the dimensional stability and architecture of collagen gels upon exposure to NaOH.

a, To study the dimensional stability of features in collagen, we polymerized collagen gels around acupuncture needles (160 μm diameter; see Methods). After polymerizing collagen, we withdrew the needle and added different concentrations of NaOH to the reservoirs ensuring flow through the channel, and placed devices on a hot plate maintained at 32 °C for 30 mins. **b,** Post NaOH treatment, we imaged these collagen gels using second harmonic generation (SHG) imaging. Until 20 mM NaOH treatment the dimension of the channel closely matched the size of the acupuncture needles and the quantification of the collagen intensity showed clear boundaries (see arrows). After 30 min exposure to 50 mM NaOH, the gels lost their structural integrity leading to broadening of the features. Gels treated with 100 mM NaOH did not show clear edges and dimensions of the channels could not be measured (not shown here). **c,** Quantification of the channel dimensions post-exposure to different concentrations of NaOH for 30 min (mean ± s.d. across 5 devices per concentration). **d,** Collagen architecture post 30-min exposure to NaOH as observed through SHG imaging of bulk collagen gels (regions shown are 100μm × 100μm). **e,** Collagen intensity changes in response to different concentration of NaOH post 30-min exposure normalized with respect of the PBS control (mean ± s.d. across 18 measurements from 6 devices per concentration).

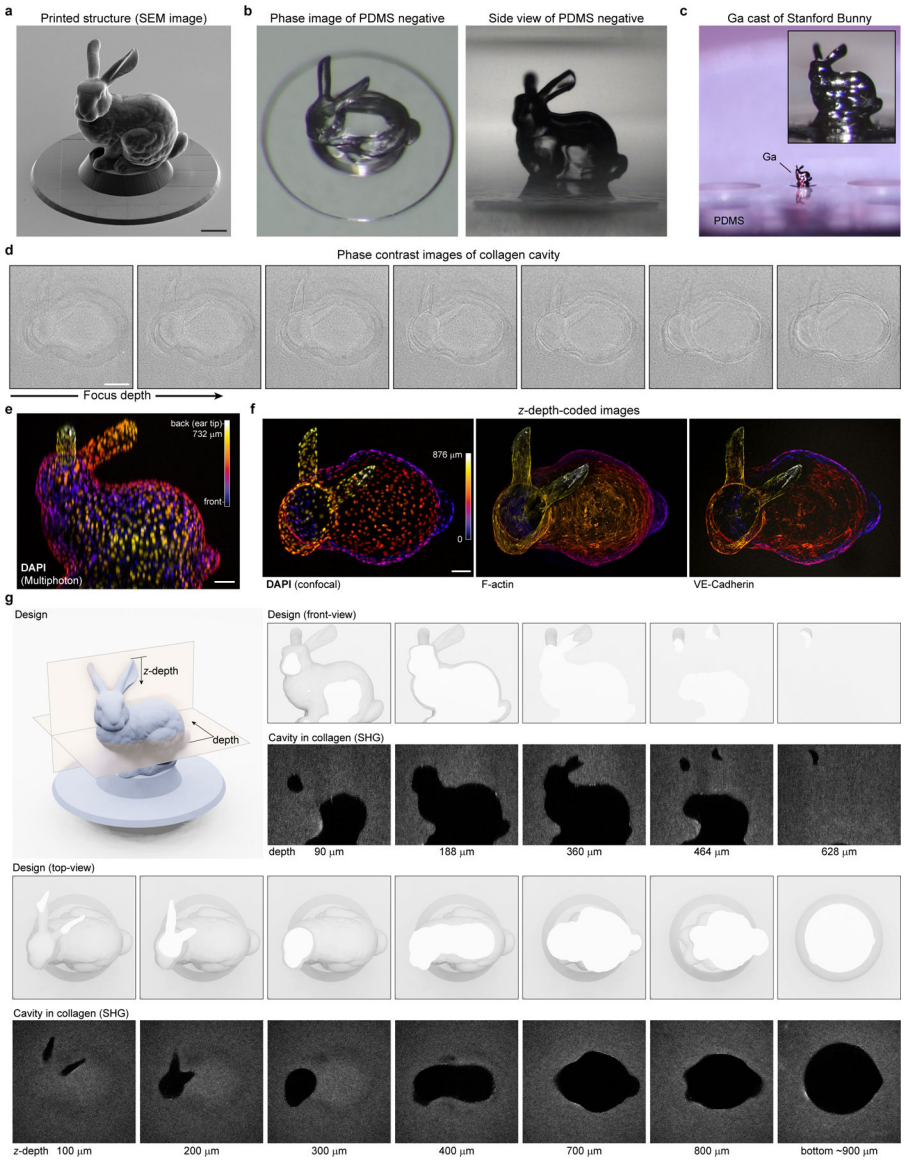

Extended Data Fig. 2 |. 3D cavities in collagen.

a, Printed Stanford Bunny. **b,** PDMS negative. **c,** Solid Ga cast. **d,** Cavity in collagen. **e,** Depth-coded projection of cell nuclei post cell seeding. **f,** Confocal image projections of DAPI, F-actin and VE-cadherin. **g,** Comparison of 3D design (sections shown in white) and the fabricated cavity (collagen SHG signal). Scale bars: **a**,**d** - 200 μm; **e**,**f** - 100 μm.

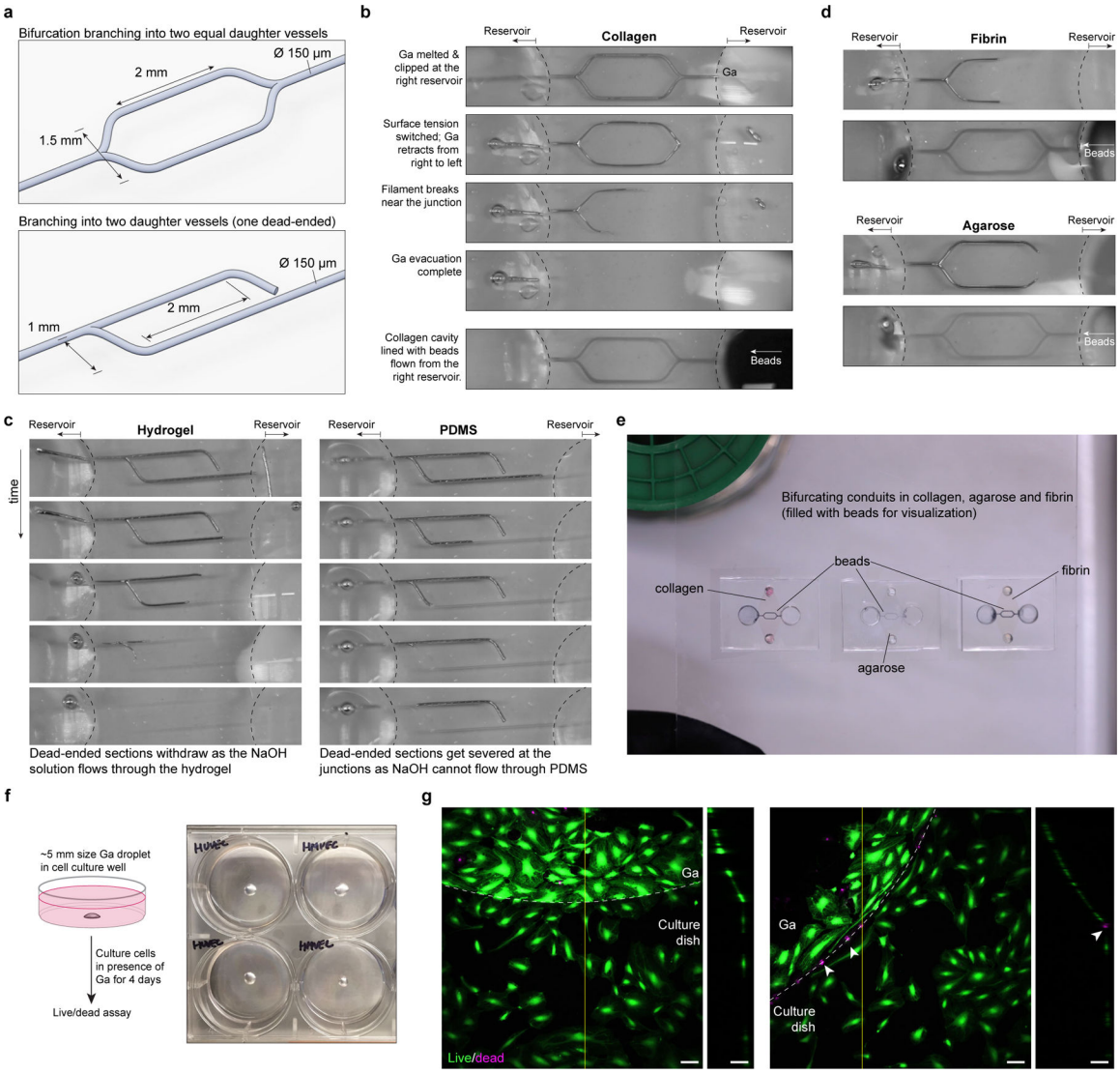

Extended Data Fig. 3 |. Capillary pumping (Ga ESCAPE) in different materials.

a, Design of bifurcations for making Ga casts. **b,** Ga can be evacuated in soft materials such as collagen. Upon removing the Ga cast, the empty cavity can be filled with cells or other materials; here the branching conduits is filled with colored beads for visualization. **c,** Geometries with both flow-accessible conduits and dead ends can be retracted at once. Critically, this differs from using Ga as a sacrificial material with non-porous surrounding materials (e.g., PDMS) without interstitial flow where dead-ended branches are severed during evacuation. **d,** Retraction process works in other soft hydrogels like fibrin or agarose. **e,** Photographs of devices with different materials upon Ga retraction with colored beads lining the conduits. **f,** Culturing cells in direct contact with Ga does not result in cell toxicity. **g,** Cells grow on top of Ga (likely on the native oxide layer) when cultured on dishes containing Ga droplets (scale bars 100 µm). Dead cells could be seen occasionally (marked by white arrows on the right) at the contact line between Ga and the culture dish which, we posit, is from the increased mechanical movement of the interface at the contact line.

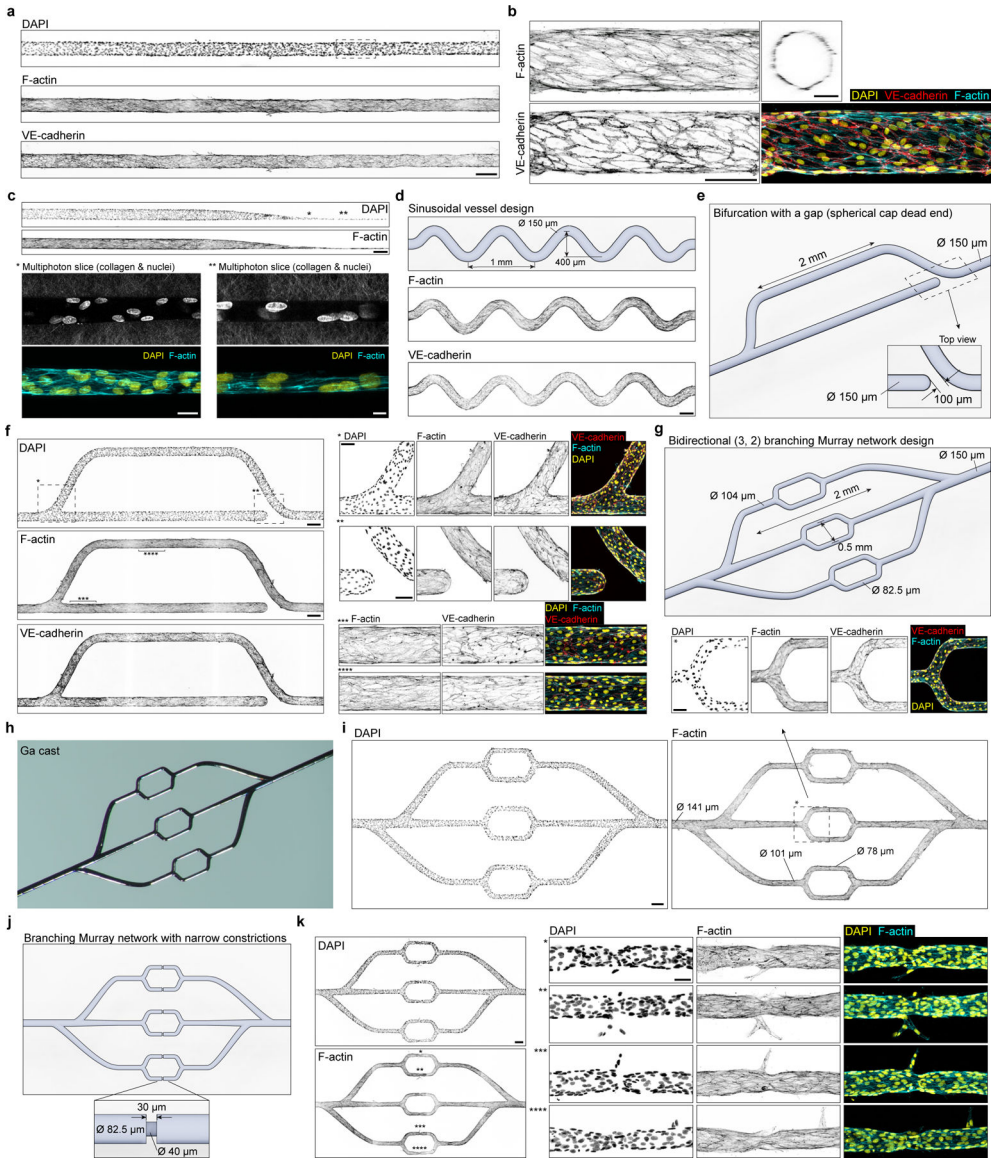

Extended Data Fig. 4 |. Endothelialized vessels.

a, 150 μm diameter cylindrical vessel seeded with endothelial cells (scale bar 200 μm). **b,** Close-up of the vessel showing F-actin and VE-cadherin (scale bar 100 μm) and the cross-section (scale bar 50 μm). **c,** Tapered vessel with caliber decreasing from 150 μm to 20 μm (scale bar 200 μm). Close-up multiphoton images show collagen and the cell nuclei in a single plane. Corresponding confocal maximum projections show that cells line the vessels uniformly until the cavity is comparable in size to the cell nuclei (scale bars: left 25 μm, right 10 μm). **d,** Sinusoidal vessel design and fabricated device (scale bar 200 μm). **e,** Bifurcating vessel with one dead-ended branch and maximum projections of the fabricated device (**f,** tile scan; scale bar 200 μm). The close-up images show the perfused and the dead-ended sections. **g,** Two-level branching Murray design (scale bar 200 μm): **h,** Ga cast and **i,** immunofluorescence images. **j,** The two-level branching design with narrow

constrictions in the smallest branches, and the fabricated device (**k,** scale bar 200 μm). Close-up images show 4 constricted sections (scale bar 50 μm).

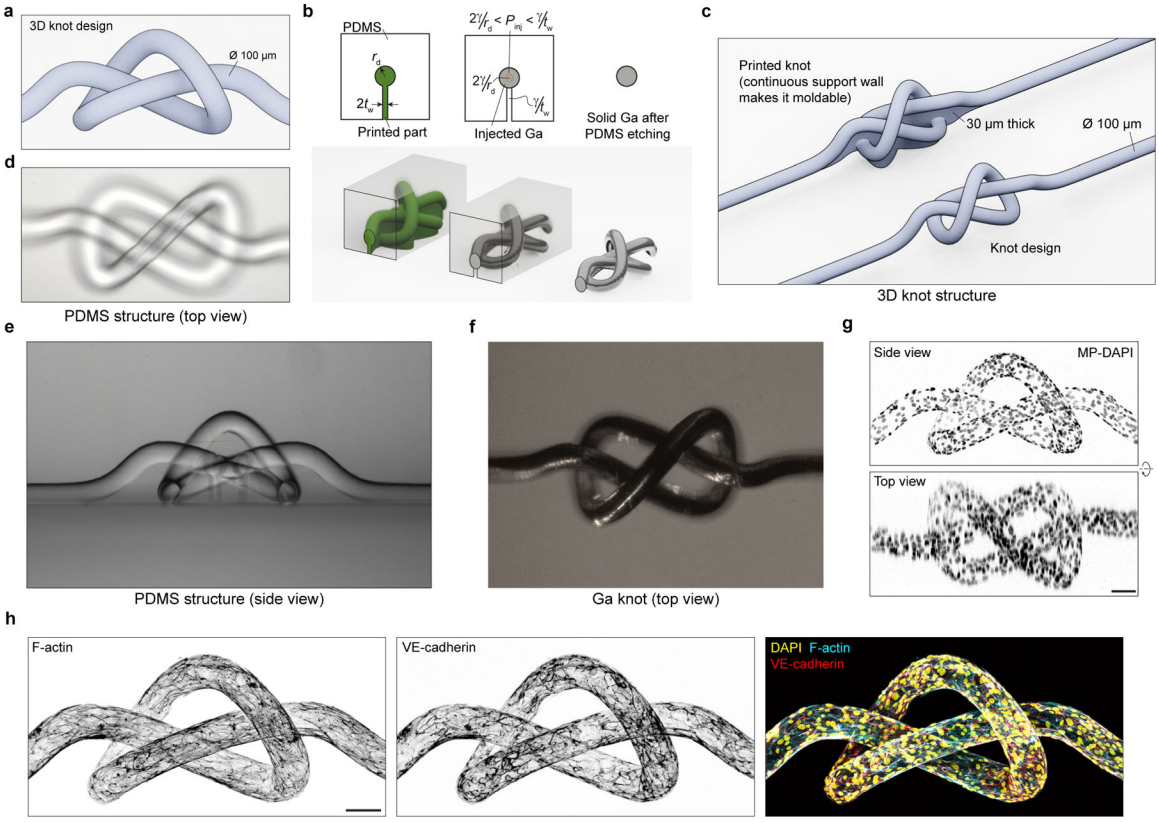

Extended Data Fig. 5 |. Self-intersecting structures.

a, 3D knot design. **b,** By introducing a narrow continuous wall under the part, self-intersecting structures such as the knot can be molded. The thickness of the wall is made to be much smaller than the feature. After demolding the negative structure, the high surface tension of the liquid is used in controlling where Ga flows, i.e., the injection pressure is above the value required to inject Ga into the knot itself but not sufficiently high for entering the gap left by the narrow wall. **c,** The modified design of the knot used for printing and the resulting shape of the Ga cast. **d,** PDMS negative copy of the printed structure (sideview in **e**). **f,** Photo of the molded Ga knot. **g,** Side- and top-view of the cell nuclei (scale bar 100 μm). **h,** Immunofluorescence images of the endothelial cell lined knot labelling F-actin and VE-cadherin (scale bar 100 μm).

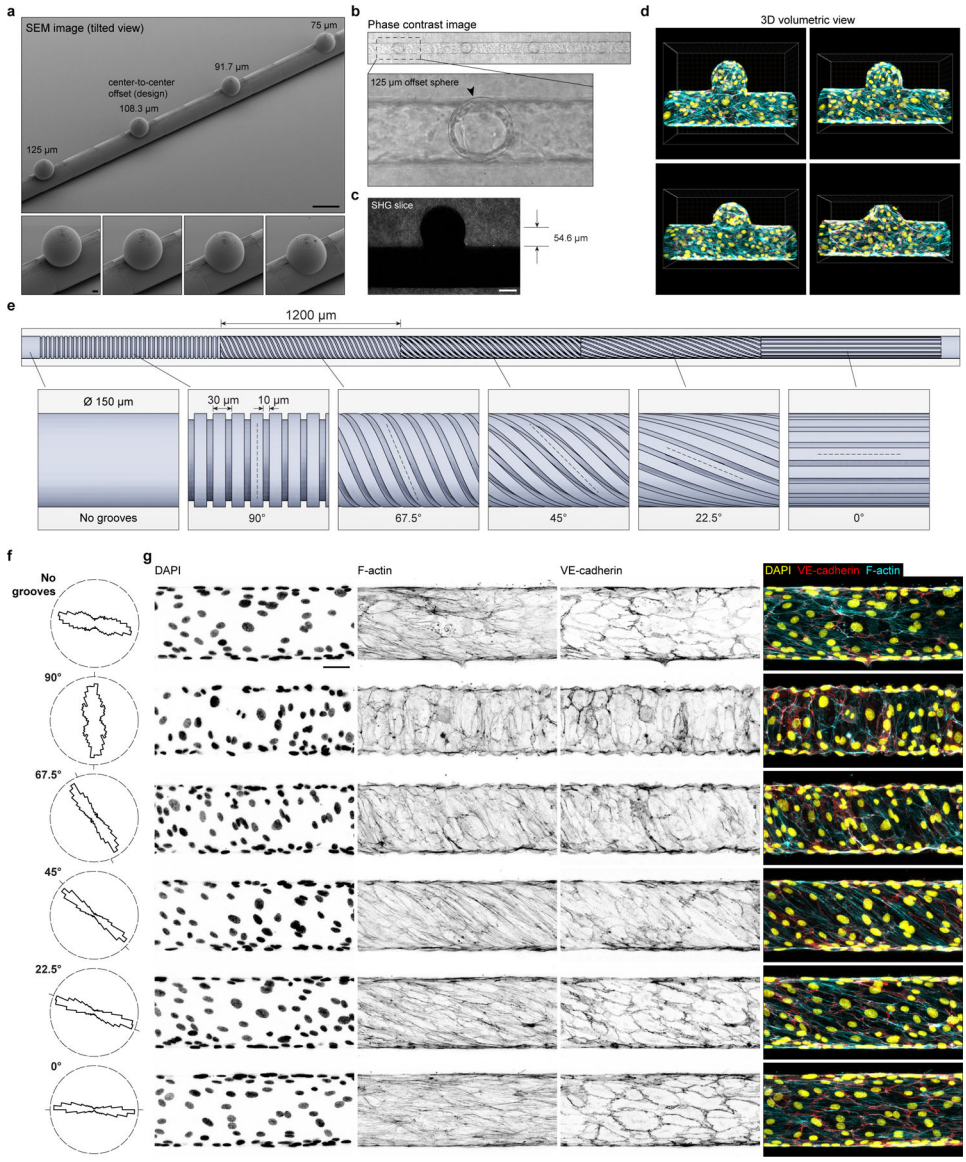

Extended Data Fig. 6 |. Fine control of vascular structures—vascular malformations and microgrooves to control cell alignment.

a, Tilted angle SEM images of the printed vascular malformation design (scale bar 200 µm). Close-up images show spherical blebs with different offsets (scale bar 20 µm). **b,** Phase contrast image of the collagen device seen from top of the blebs. The fabrication process yields high resolution, smooth spherical blebs (shown by the arrow). **c,** SHG slice of collagen (averaged) through one bleb structure prior to cell seeding (scale bar 50 µm). **d,** 3D volumetric views of the different spherical blebs. **e,** Design of a cylindrical vessel with no orientation cues and 5 regions to align cells progressively from 90° to 0° (along the length of the vessel). **f,** Orientation histograms of the cells (F-actin) at different regions of the vessel. **g,** Half vessel maximum projections of DAPI, F-actin and VE-cadherin at different vessel regions (scale bar 50 µm).

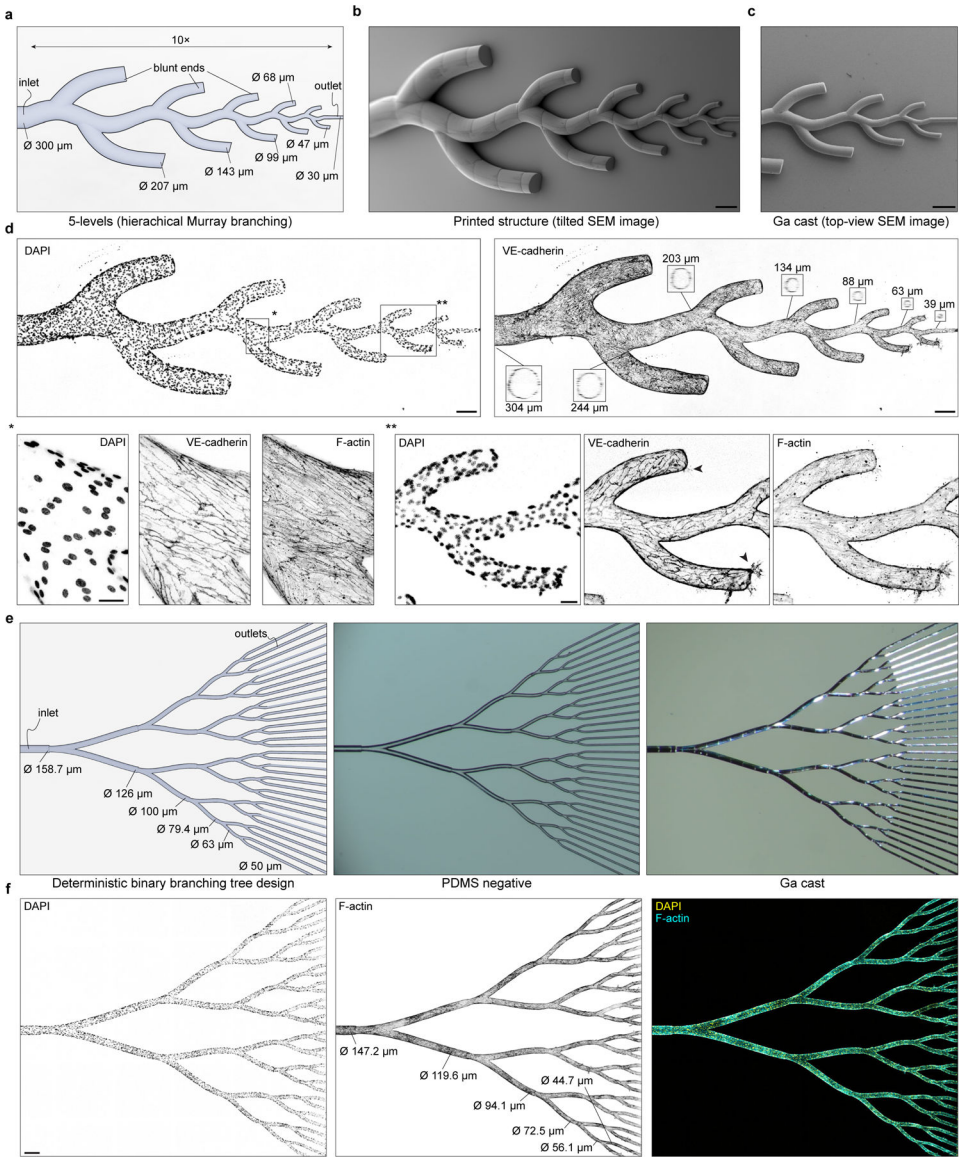

Extended Data Fig. 7 |. Hierarchical branching trees with both perfused and dead-ended sections.

a, Branching vessel architecture with a 10-fold reduction in vessel caliber. The vessels are dimensioned according to Murray's law (with exponent 2.96) at each branching hierarchy. **b,** Tilted-angle SEM images of the printed structure. Scale bar 200 µm. **c,** SEM image of the smallest branches of the Ga cast. **d,** Tile scan of the device showing the cell nuclei and VE-cadherin. The insets show vessel cross-sections at different regions of the device. Scale bar 200 µm. The close-up images (bottom) show a branch point and cells sprouting from the blunt ends at ~60 µm sized vessels. Scale bars 50 µm. **e,** Design of a deterministic tree with symmetric bifurcations with each vessel (perfusable). **f,** Maximum projection of tile scans of the deterministic binary tree. Scale bar 250 µm.

Extended Data Fig. 8 |. Computationally generated vascular trees.

To generate complex vascular trees, we computationally generated trees loosely inspired by natural signaling (space colonization algorithm[37,38]). Cells are virtually distributed in space and the vascular network is grown to nourish these virtual cells by approaching a distance less than a defined diffusion length (called vessel-cell distance, VCD). The generated vascular tree skeleton is then subsequently sized according to branching laws such as Murray's law. The influence of key parameters of our algorithm is shown here; see Methods for more details. Increasing the cell number (*N*) increases the number of branches. The distance of influence (DOI) defines the distance within which cells influence the growth of specific nodes of the tree. Increasing the DOI causes more cells to direct tree growth causing the final tree to have more directed branching. VCD is analogous to the diffusion distance and dictates how closely a vessel must approach a cell to nourish it. Increasing the VCD implies that vessels can successfully transport nutrients to far-away cells resulting in a

sparse tree with fewer branches spaced far apart. Step size is the distance by which the tree is grown in the algorithm, and tortuosity factor is a multiplier that adds random fluctuations to the vector determining the tree branching angles; see Methods for more details.

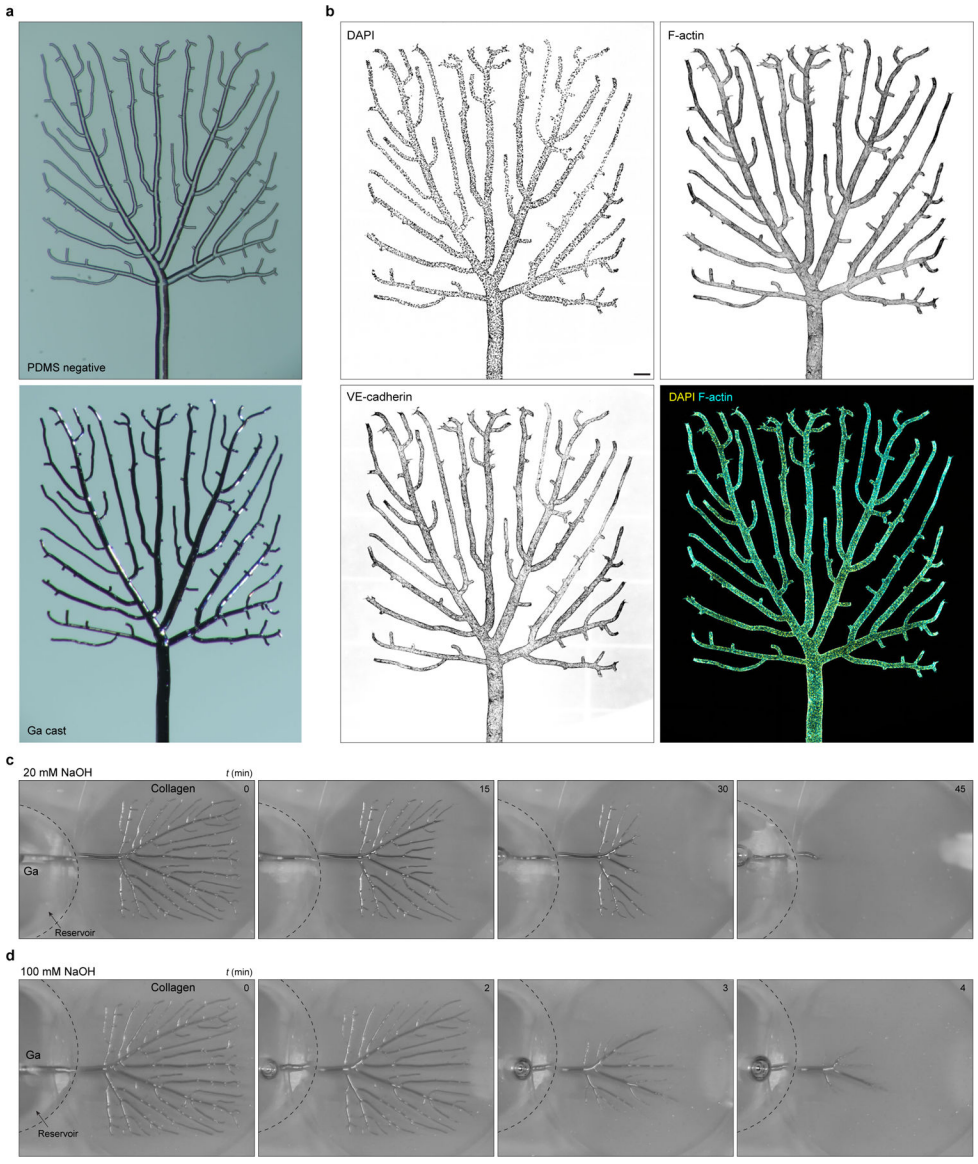

Extended Data Fig. 9 |. Rectangular tree.

a, PDMS negative of the 4 × 4 mm^2 tree. **b,** Tile scan of the vascular tree showing the cell nuclei and F-actin. Scale bar 250 μm. **c,** Time course images of the Ga retraction process with 20 mM NaOH (see Supplementary Video 12). **d,** When high concentrations of NaOH are used, the retraction process is expedited, showing that the retraction rate is determined by how the surface oxide is removed (spatially) and not limited by the evacuation rate of liq. Ga through the central root.

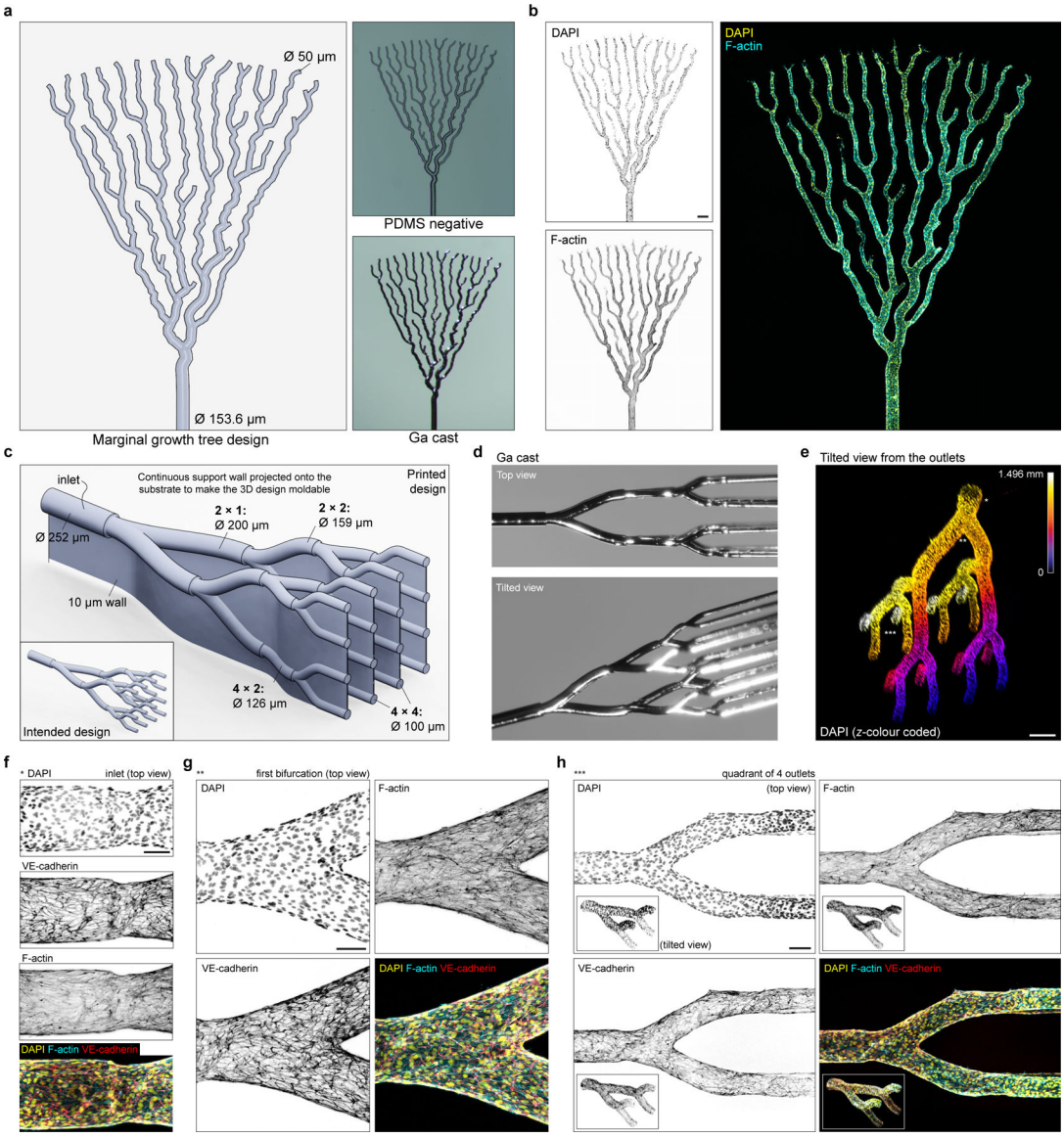

Extended Data Fig. 10 |. Marginal growth and hierarchical 3D vascular trees.

a, Design generated through marginal growth (where the boundary is grown iteratively; see Methods), the corresponding PDMS negative and the Ga cast. **b,** Tile scan of the marginal growth tree showing F-actin and DAPI. Scale bar 250 µm. **c,** Hierarchical 3D vascular tree design branching from 1 inlet to 16 outlets with the branches sized per Murray's Law. The projected thin support wall (10 µm thick) makes the printed 3D structure moldable, i.e., PDMS can be polymerized around this structure and removed. Subsequently, when liq. Ga is injected into the mold, it preferentially fills the branching vascular structure (all features >> 10 µm) but not the narrow wall yielding a cast of the intended design. **d,** Photographs of the gallium cast as viewed from the top and when tilted. **e,** Tilted (volumetric) view of the cell nuclei of the endothelial monolayer through SHG imaging as viewed from the array of outlets; colour denotes the vertical position. Scale bar 300 µm. Maximum projections of the inlet (**f**), the first bifurcation (**g**), and a quadrant of outlets (**h**) showing DAPI, VE-cadherin

and F-actin. Scale bars 100 μm. The insets in **h** show the corresponding regions in a titled volumetric view. The regions shown in **f**, **g**, and **h** are marked in the full device image (**e**) as *, **, and *** respectively.

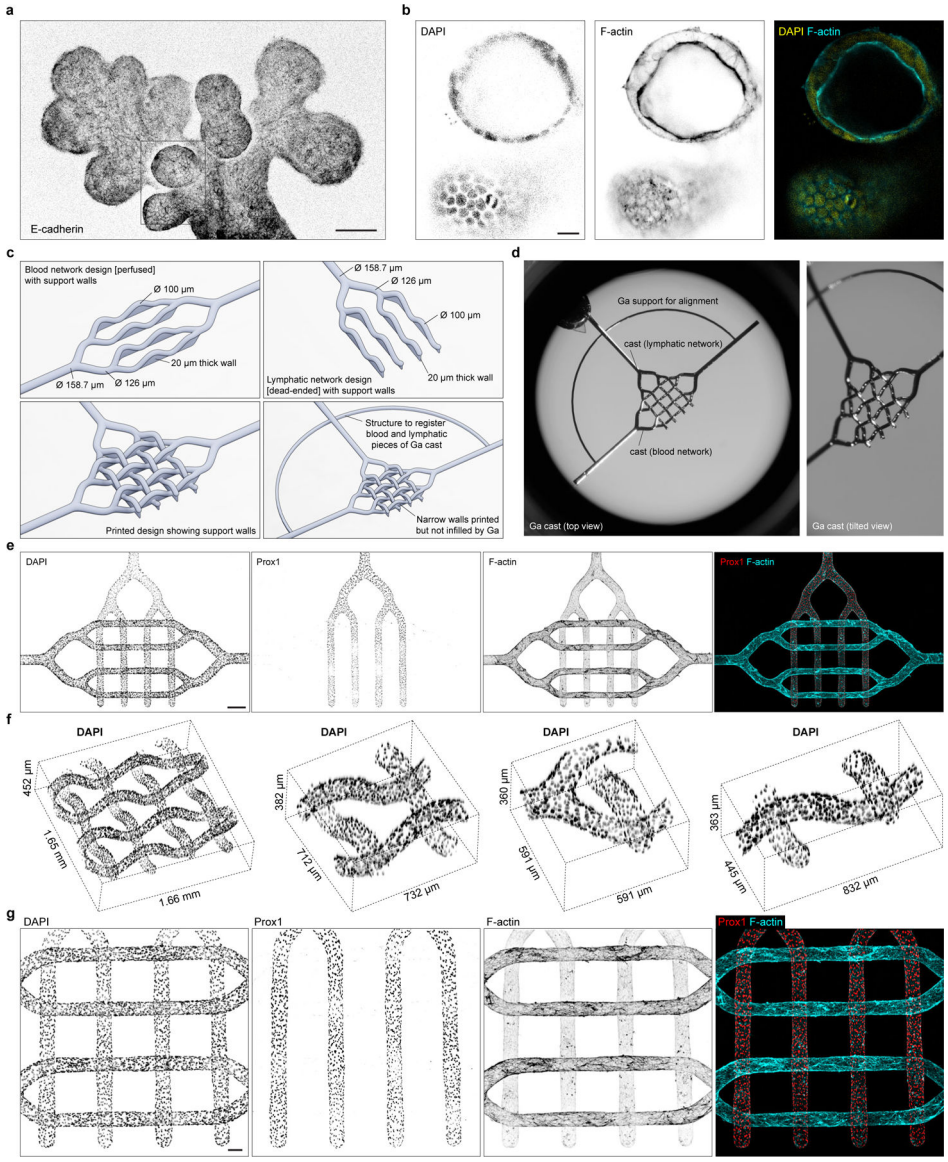

Extended Data Fig. 11 |. Applications—epithelial buds and orthogonal (blood and lymphatic) networks.

a, Maximum projection of the 3D epithelial bud geometry (E-cadherin). Scale bar 100 μm. The close-up images show the cell nuclei and F-actin at a slice through a single bud. Scale bar 20 μm. **b,** Design of the 3D, enmeshed blood and lymphatic networks and supporting structures. **c,** The enmeshed architecture requires thin support walls (20 μm thick) projected onto the substrate to make the design moldable. The Ga pieces corresponding to the blood and lymphatic network are aligned with respect to each other through a supporting arc (outside the device/gel region). **d,** Ga cast. **e,** Maximum projections of the device (scale bar

300 μm). Volumetric (**f**) and close up projections (**g**; scale bar 100 μm) of the enmeshed parts of the device (see Fig 4b–4d).

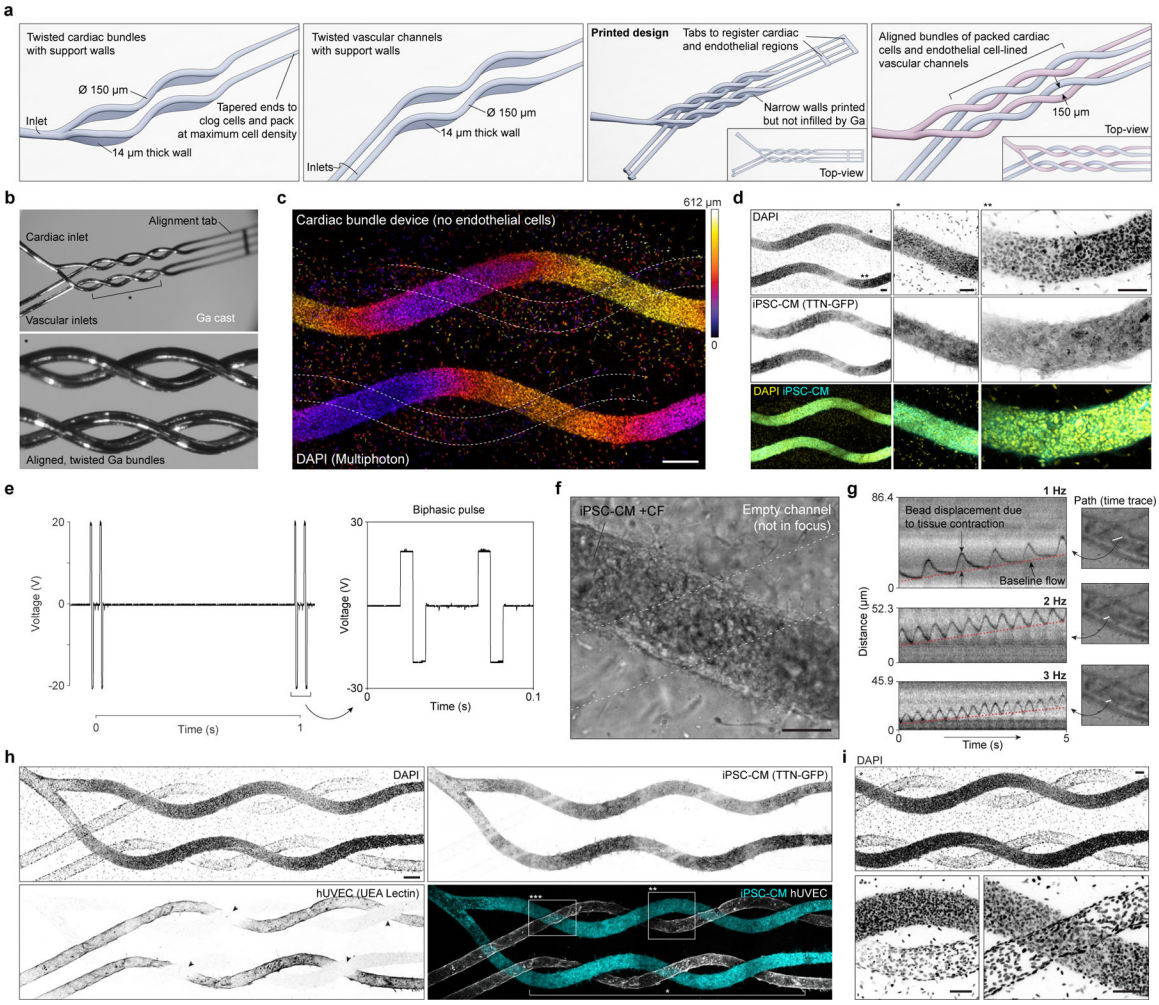

Extended Data Fig. 12 |. Cardiac bundles with vasculature.

a, Design consists of helical cardiac bundles maximally packed with iPSC-derived cardiomyocytes (iPSC-CM; 90%) and cardiac fibroblasts (CF; 10%) twisted along with aligned vascular channels separated by 150 μm. Thin supporting walls projected onto the substrate (14 μm) are used to make the design moldable. Tabs at the right end hold the cardiac and vascular portions of the Ga cast together at the ends of the cast. **b,** Ga casts of the twisted cardiac and vascular regions. **c,** To study the effectiveness of maximally packing cells in the cardiac portions, devices we filled with a mixture of iPSC-CMs (90%) and CFs (10%) in the cardiac portions alone and the vascular regions were left empty. Depth-coded projection of the cell nuclei (scale bar 200 μm). **d,** The iPSC-CMs are confined to bundles and the cells in the bulk are cardiac fibroblasts as seen in the maximum projection images (scale bar 100 μm). **e,** Voltage waveforms used for 1 Hz electrical stimulation and a close-up of the biphasic pulse. **f,** Phase image of the device region showing the cardiac bundle and the vascular channel with beads (not in focus). Scale bar 100 μm. **g,** Upon the addition of tracer beads into the vascular conduit, the displacement of particles can be tracked along

specific paths in the form of kymographs (see Supplementary Video 15). The beads appear as black spots forming traces that show the baseline flow rate from the pressure head and the impact of cardiac contraction at different stimulations frequencies. **h,** Maximum projections of the devices containing both cardiac cells (in the cardiac portions) and a confluent layer of endothelial cells in the vascular conduits. Scale bar 200 μm. **i,** Close-up images showing the cell nuclei of regions marked in **h** and corresponding to Fig. 4g (scale bars 100 μm).

Supplementary Material

Refer to Web version on PubMed Central for supplementary material.

Acknowledgements

S.S. thanks Herbert Shea and Ryan C. Hayward for their comments and discussions. We gratefully acknowledge support from the NIH National Institute of Biomedical Imaging and Bioengineering (NIH-EB00262, NIH-EB033821), National Science Foundation Engineering Research Center on Cellular Metamaterials (EEC-1647837), National Science Foundation Science and Technology Center for Engineering Mechano-Biology (CMMI-1548571), Allen Distinguished Investigator Program, U.S.-Israel Binational Science Foundation (BSF 2017239), American Heart Association Postdoctoral Fellowship (20POST35210045), NIH National Heart Lung and Blood Institute (F31HL156517), NIH T32 Quantitative Biology and Physiology training grant, and the Portuguese Foundation for Science and Technology (FCT; doctoral grant SFRH/BD/129224/2017).

Data availability.

The main data supporting the findings in this study are available within the main text, methods, and supplementary information. Other data generated or analyzed are available from the corresponding authors on request.

References

1. Weibel ER It takes more than cells to make a good lung. American Journal of Respiratory and Critical Care Medicine 187, 342–346 (2013). [PubMed: 23418327]
2. Buckberg G, Hoffman JIE, Mahajan A, Saleh S & Coghlan C Cardiac mechanics revisited: The Relationship of Cardiac Architecture to Ventricular Function. Circulation 118, 2571–2587 (2008). [PubMed: 19064692]
3. Grigoryan B et al. Multivascular networks and functional intravascular topologies within biocompatible hydrogels. Science 364, 458–464 (2019). [PubMed: 31048486]
4. Lee A et al. 3D bioprinting of collagen to rebuild components of the human heart. Science 365, 482–487 (2019). [PubMed: 31371612]
5. Skylar-Scott MA et al. Biomanufacturing of organ-specific tissues with high cellular density and embedded vascular channels. Science Advances 5, (2019).
6. McKinnon DD, Brown TE, Kyburz KA, Kiyotake E & Anseth KS Design and characterization of a synthetically accessible, photodegradable hydrogel for user-directed formation of neural networks. Biomacromolecules 15, 2808–2816 (2014). [PubMed: 24932668]
7. Brandenberg N & Lutolf MP In situ patterning of microfluidic networks in 3D cell-laden hydrogels. Advanced Materials 28, 7450–7456 (2016). [PubMed: 27334545]
8. Arakawa CK, Badeau BA, Zheng Y & DeForest CA Multicellular vascularized engineered tissues through user-programmable biomaterial photodegradation. Advanced Materials 29, 1703156 (2017).
9. Daly AC, Prendergast ME, Hughes AJ & Burdick JA Bioprinting for the biologist. Cell 184, 18–32 (2021). [PubMed: 33417859]
10. Pradhan S, Keller KA, Sperduto JL & Slater JH Fundamentals of laser-based hydrogel degradation and applications in Cell and Tissue Engineering. Advanced Healthcare Materials 6, 1700681 (2017).

11. O'Connor C, Brady E, Zheng Y, Moore E & Stevens KR Engineering the multiscale complexity of vascular networks. Nature Reviews Materials 7, 702–716 (2022). [PubMed: 35669037]
12. Traore MA & George SC Tissue Engineering the Vascular Tree. Tissue Engineering Part B: Reviews 23, 505–514 (2017). [PubMed: 28799844]
13. Truby RL & Lewis JA Printing soft matter in three dimensions. Nature 540, 371–378 (2016). [PubMed: 27974748]
14. Zheng X et al. Ultralight, ultrastiff mechanical metamaterials. Science 344, 1373–1377 (2014). [PubMed: 24948733]
15. Keating SJ, Leland JC, Cai L & Oxman N Toward site-specific and self-sufficient robotic fabrication on architectural scales. Science Robotics 2, (2017).
16. Xing J-F, Zheng M-L & Duan X-M Two-photon polymerization microfabrication of Hydrogels: An advanced 3D printing technology for Tissue Engineering and drug delivery. Chemical Society Reviews 44, 5031–5039 (2015). [PubMed: 25992492]
17. Bellan LM, Singh SP, Henderson PW, Porri TJ, Craighead HG & Spector JA Fabrication of an artificial 3-dimensional vascular network using sacrificial sugar structures. Soft Matter 5, 1354–1357 (2009)
18. Kolesky DB, Homan KA, Skylar-Scott MA & Lewis JA Three-dimensional bioprinting of thick vascularized tissues. Proceedings of the National Academy of Sciences 113, 3179–3184 (2016).
19. Jiménez-Torres JA, Peery SL, Sung KE & Beebe DJ LumeNEXT: A practical method to pattern luminal structures in ECM Gels. Advanced Healthcare Materials 5, 198–204 (2015). [PubMed: 26610188]
20. Miller JS et al. Rapid casting of patterned vascular networks for perfusable engineered three-dimensional tissues. Nature Materials 11, 768–774 (2012). [PubMed: 22751181]
21. Zheng Y et al. In vitro microvessels for the study of angiogenesis and thrombosis. Proceedings of the National Academy of Sciences 109, 9342–9347 (2012).
22. Lin Y et al. Vacuum filling of complex microchannels with Liquid Metal. Lab on a Chip 17, 3043–3050 (2017). [PubMed: 28805880]
23. Deng F, Nguyen Q-K & Zhang P Multifunctional liquid metal lattice materials through hybrid design and manufacturing. Additive Manufacturing 33, 101117 (2020).
24. Hwang D, Barron EJ III, Haque AT & Bartlett MD Shape morphing mechanical metamaterials through reversible plasticity. Science Robotics 7, eabg2171 (2022). [PubMed: 35138882]
25. Tang S-Y, Tabor C, Kalantar-Zadeh K & Dickey MD Gallium Liquid Metal: The devil's elixir. Annual Review of Materials Research 51, 381–408 (2021).
26. Khan MR, Eaker CB, Bowden EF & Dickey MD Giant and switchable surface activity of liquid metal via surface oxidation. Proceedings of the National Academy of Sciences 111, 14047–14051 (2014).
27. Ma J et al. Shaping a soft future: Patterning liquid metals. Advanced Materials 35, 19 (2023).
28. Pourbaix M Atlas of Electrochemical Equilibria in aqueous solutions. (NACE International, 1974).
29. Hardy SC The surface tension of liquid gallium. Journal of Crystal Growth 71, 602–606 (1985).
30. Walker GM & Beebe DJ A passive pumping method for microfluidic devices. Lab on a Chip 2, 131 (2002). [PubMed: 15100822]
31. Style RW, Jagota A, Hui C-Y & Dufresne ER Elastocapillarity: Surface tension and the mechanics of soft solids. Annual Review of Condensed Matter Physics 8, 99–118 (2017).
32. Bico J, Reyssat É & Roman B Elastocapillarity: When surface tension deforms elastic solids. Annual Review of Fluid Mechanics 50, 629–659 (2018).
33. Polacheck WJ, Kutys ML, Tefft JB & Chen CS Microfabricated blood vessels for modeling the Vascular Transport Barrier. Nature Protocols 14, 1425–1454 (2019). [PubMed: 30953042]
34. Murray CD The physiological principle of minimum work. Proceedings of the National Academy of Sciences 12, 207–214 (1926).
35. Sherman TF On connecting large vessels to small: the meaning of Murray's law. The Journal of general physiology 78, 431–453 (1981). [PubMed: 7288393]
36. Wang C, Baker BM, Chen CS & Schwartz MA Endothelial cell sensing of Flow Direction. Arteriosclerosis, Thrombosis, and Vascular Biology 33, 2130–2136 (2013). [PubMed: 23814115]

37. Runions A et al. Modeling and visualization of leaf venation patterns. ACM Transactions on Graphics 24, 702–711 (2005).

38. Runions A, Lane B & Prusinkiewicz P Modeling trees with a space colonization algorithm. In Proc. 3rd Eurographics Workshop on Natural Phenomena, 63–70 (2007).

39. Oliver G, Kipnis J, Randolph GJ & Harvey NL The lymphatic vasculature in the 21st century: novel functional roles in homeostasis and disease. Cell 182, 270–296 (2020). [PubMed: 32707093]

40. Doyle AD Generation of 3D collagen gels with controlled diverse architectures. Current Protocols in Cell Biology 72, 1 (2016).

41. Song H-H, Greco A, Lammers S, Sundaram L, Rubio AX, Chen L, Li J, Eyckmans J, Bhatia SN & Chen CS Transient support from fibroblasts is sufficient to drive functional vascularization in engineered tissues. Advanced Functional Materials 30, 2003777 (2020). [PubMed: 33613149]

42. Lian X et al. Directed cardiomyocyte differentiation from human pluripotent stem cells by modulating Wnt/β-catenin signaling under fully defined conditions. Nature Protocols 8, 162–175 (2013). [PubMed: 23257984]

43. Zhang K, Cloonan PE, Sundaram S, Liu F, Das SL, Ewoldt JK, Bays JL, Tomp S, Toepfer CN, Marsiglia JD & Gorham J Plakophilin-2 truncating variants impair cardiac contractility by disrupting sarcomere stability and organization. Science Advances 7, eabh3995 (2021). [PubMed: 34652945]

44. Bilodeau RA, Zemlyanov DY & Kramer RK Liquid metal switches for environmentally responsive electronics. Advanced Materials Interfaces 4, 1700126 (2017).

45. Kleiman M, Ryu KA & Esser-Kahn AP Determination of factors influencing the wet etching of polydimethylsiloxane using tetra-n-butylammonium fluoride. Macromolecular Chemistry and Physics 217, 284–291 (2015).

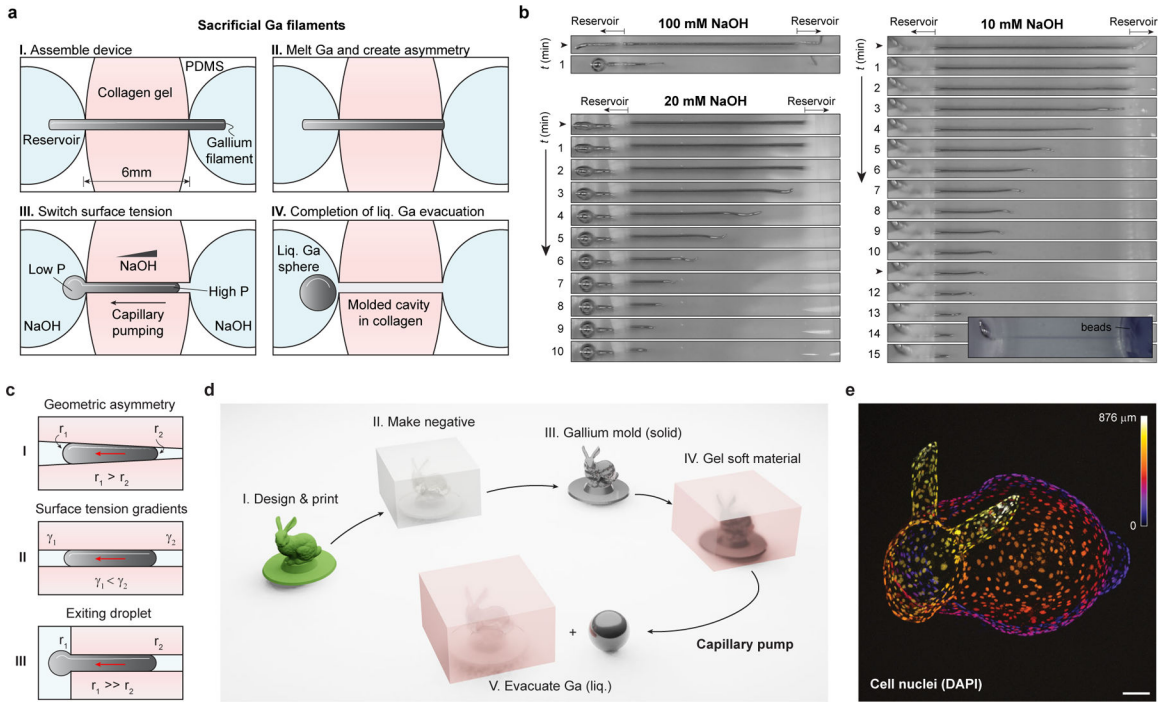

Fig. 1 |. Capillary pumps for sacrificial molding.

a, We assemble gallium filaments (150 µm diameter) into a PDMS device after which collagen is added and polymerized in central gel region surrounding the filament. Two open reservoirs offer direct access to the gallium filament. We subsequently raise the temperature to melt gallium, and sever one of the exposed sections of the liquid filament (right reservoir in schematic) to create a geometric asymmetry. When the surface tension is raised by removing the native surface oxide of gallium, the liquid plug evacuates to the side with the larger exposed gallium section (due to its lower Laplace pressure), eventually forming a fully-evacuated sphere. **b,** When 100 mM NaOH is used for gallium evacuation, the entire length of the device is retracted in ~1 min and at times uncontrollably breaking the plug into multiple pieces. A controlled, gradual evacuation was observed when 20 mM and 10 mM NaOH were used; see Supplementary Videos 2–5. The arrows in the time axis indicate when fresh NaOH solution was added. Inset shows dark colored beads added to the cylindrical cavity for visualization. **c,** The Laplacian pressure across an interface is determined by the surface tension (γ) and the principal curvatures (r^{-1}). When a high surface tension droplet is physically constrained (with contact angle ~ 180°), the resulting differences in capillary forces can result in directional flows. In the presence of geometric asymmetries (I), e.g., with narrowing towards one direction, capillary pumps force liquids against this narrowing. Surface tension gradients (II) can result in this effect directly even in the absence of any geometric variations. When a liquid droplet exits an opening (III), the lower curvature at the exiting end of the droplet forces it to evacuate completely. **d,** Capillary pumps can be used to create high-resolution copies of multiscalar structures in soft materials, by decoupling the material used for achieving resolution and complexity from the final material of choice such as soft natural extracellular matrix (ECM) materials suitable for 3D cell culture. Engineered sacrificial capillary pumps for evacuation (ESCAPE)-molding process steps are as follows: the intended design is first fabricated using any process (I) and copied into a Ga cast through

replica molding (II & III). Soft ECMs are polymerized around the solid Ga cast (IV). At the heart of this fabrication scheme is the use of capillary pumps to extract Ga in its liquid form without disturbing the soft material (V). **e,** Upon Ga removal, cells are seeded into the Stanford Bunny shaped cavity. The image shows a depth-coded projection of cell nuclei labelled with DAPI. Scale bar 100 μm.

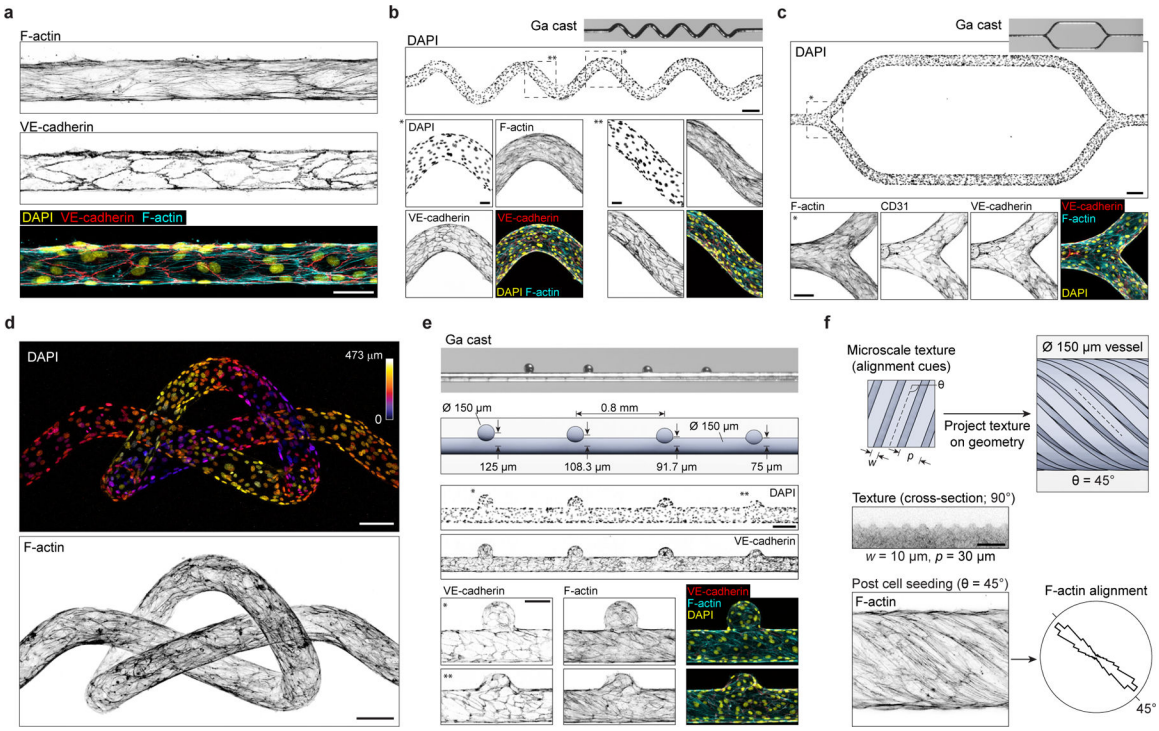

Fig. 2 |. Endothelialized structures—vessel topologies and fine features.

a, 60 μm cylindrical vessel (scale bar 50 μm). **b,** Sinusoidal vessel (scale bar 200 μm); see design in Extended Data Fig. 4. Close-ups show the curved and linear regions (scale bar 50 μm). **c,** 150 μm vessel that bifurcates into two equally sized daughter vessels (scale bar 200 μm); zoomed in sections show the branching junction (scale bar 100 μm). **d,** Geometries such as an overhand knot (100 μm diameter; see Extended Data Fig. 5) can be realized with the Ga ESCAPE molding approach (scale bar 100 μm). **e,** Vascular malformations consisting of spherical blebs offset from the cylindrical vessel (full device scale bar 200 μm; close-up projections scale bar 100 μm). **f,** Microscale texture to orient endothelial cells can be projected on the blood vessel designs to control cell alignment in addition to the overall vessel geometry. Images show the cross section of the texture (scale bar 50 μm) and a section of the vessel with grooves oriented at θ = 45° (see Extended Data Fig. 6e, 6f). Histogram shows the alignment of actin filaments in the cell.

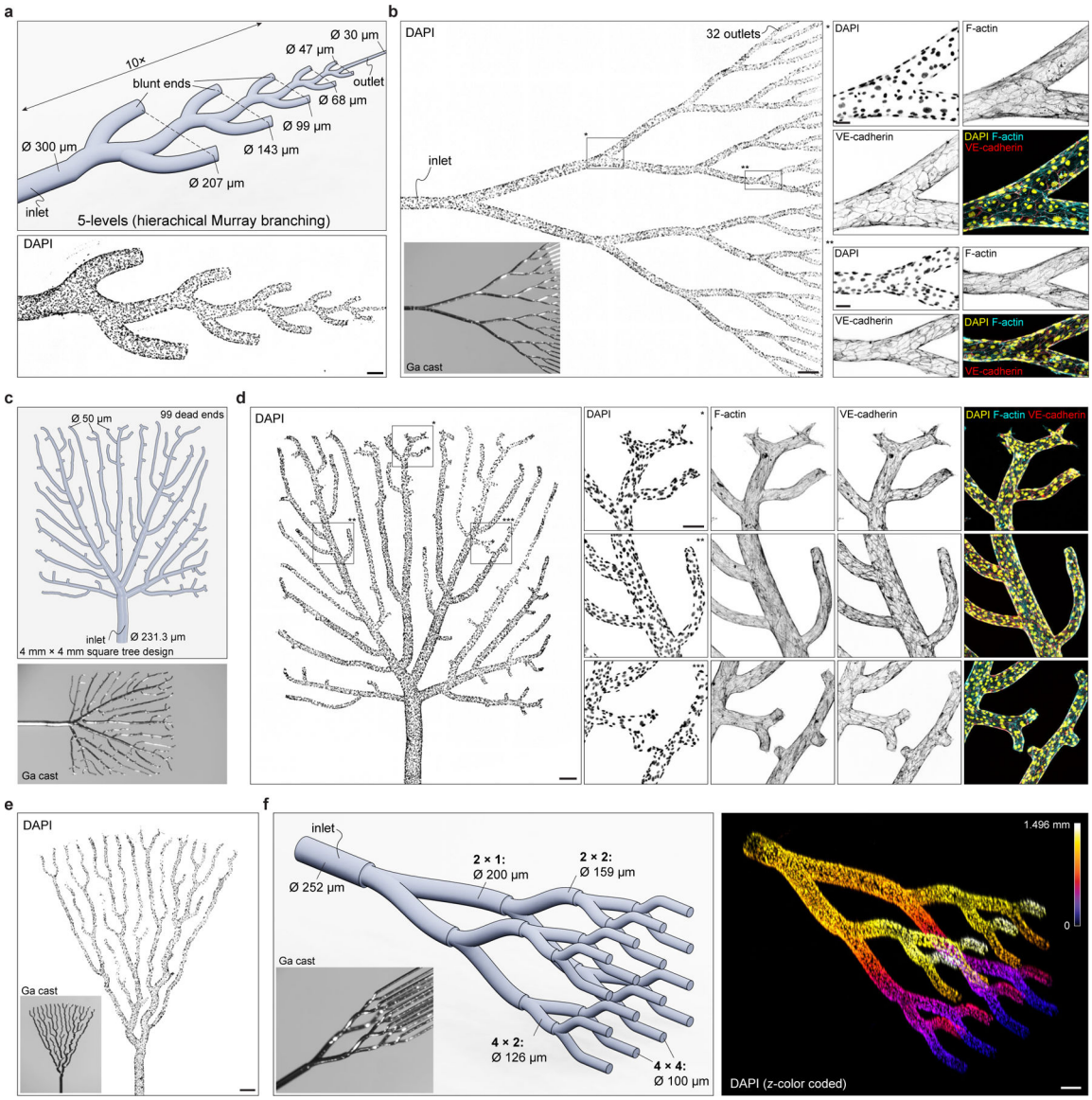

Fig. 3 |. Hierarchical vascular trees and epithelial ducts.

a, Hierarchical branching architecture with diameters spanning an order of magnitude (scale bar 200 µm). **b,** Tile scan of a binary branching tree where each vessel is subjected to flow (i.e., the design has no dead ends). Inset: Ga cast. The closeup images show branching junctions at two hierarchical levels. **c,** Computationally generated square tree covering 4mm × 4mm. Each terminal branch of the tree is set to be a 50 µm-sized (dead-ended) vessel. All higher hierarchical branches are sized according to Murray's Law resulting in an inlet diameter of 231.3 µm. The tree was grown with a distance of influence (DOI) of 1000 µm, and a vessel-cell distance (VCD) of 100 µm (see Extended Data Fig. 8 and Methods). Bottom image shows the Ga cast. **d,** Tile scan of the cell nuclei after cell seeding (scale bar 250 µm). The closeup images show portions of device where dead-ended sections come near each other and other regions of branching (scale bar 100 µm). **e,** Tile scan of a marginal growth tree (cell nuclei) designed to fit a sector of a circle, with aligned vessels (scale bar

250 μm). Inset shows the Ga cast. **f,** 3D branching vascular networks following Murray's law generated with ESCAPE. Design on the left shows 4 levels of branching starting from a single inlet to 16 perfused outlets in a 4 × 4 grid. Inset shows the Ga cast. 3D volume (right) shows the cell nuclei colour coded by *z*-value. Scale bar 200 μm.

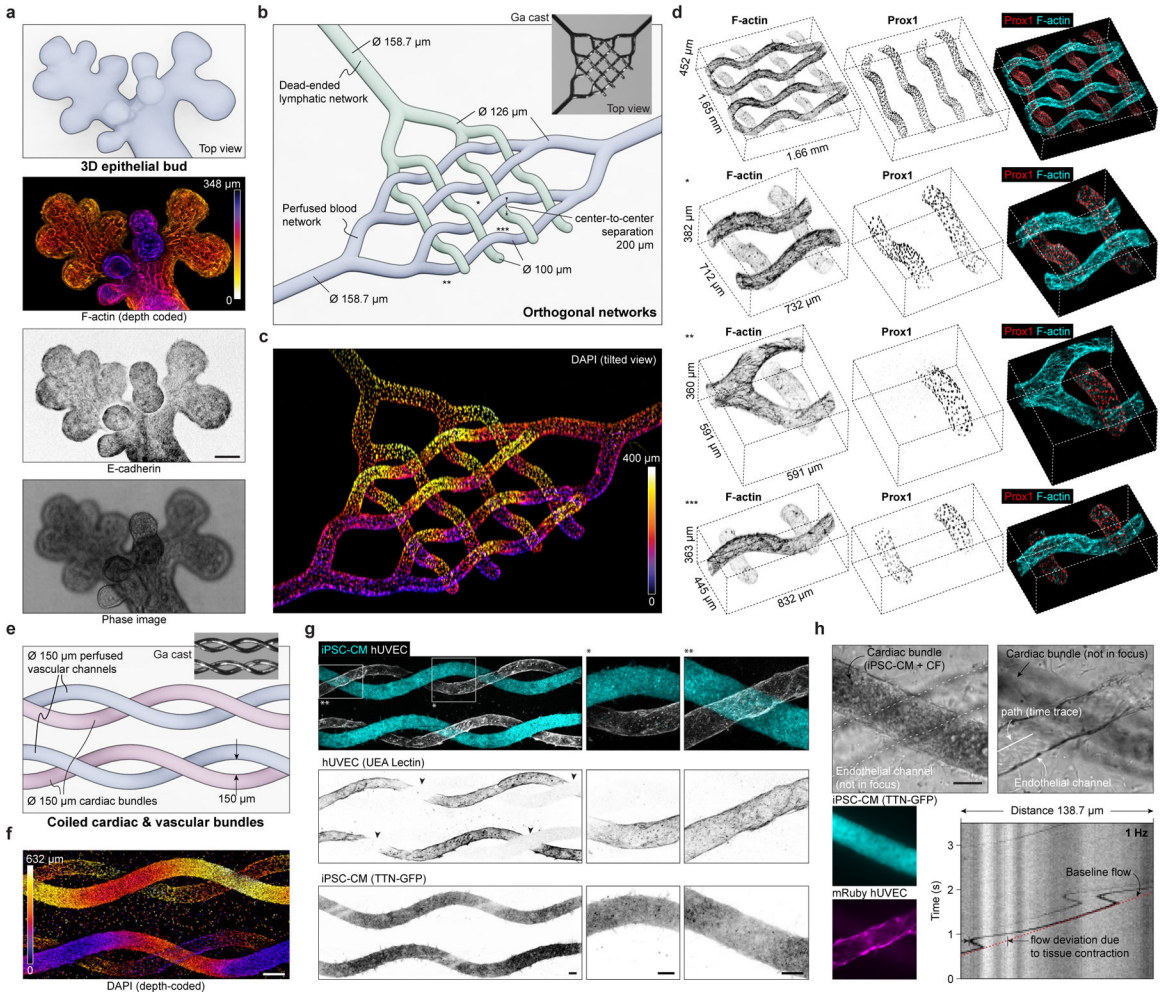

Fig. 4 |. 3D applications of ESCAPE—epithelial ducts, multicellular orthogonal networks, and cell dense structures with proximal vasculature.

a, The ESCAPE process can be expanded to non-vascular geometries such as epithelial ducts. Images show the original design of the 3D epithelial duct, depth-coded F-actin image, maximum projection of E-cadherin and a phase contrast image post epithelial cell culture, (see Extended Data Fig. 11). Scale bar 100 µm. **b,** Design of enmeshed blood (perfused) and lymphatic (dead-ended) networks and the resulting Ga cast. **c,** Cell nuclei colour coded by z-position showing the interwoven 3D geometry. **d,** Volumetric 3D view of the enmeshed regions showing all the cells (F-actin) and lymphatic cells (labelled by Prox1); corresponding DAPI images are in Extended Data Fig. 11f. **e,** Design of twisted cardiac and vascular bundles and corresponding Ga cast. **f,** The cardiac regions are maximally packed with iPSC-derived cardiomyocytes (iPSC-CMs; 90%) and cardiac fibroblasts (CFs; 10%). The vascular conduits are lined by a confluent monolayer of endothelial cells. The depth-coded DAPI image shows the helical cardiac bundles and vascular conduits. Scale bar 200 µm. **g,** Tile scans and close up images of the coiled section showing all cells, hUVECs (UEA Lectin) and iPSC-CMs (TTN-GFP); corresponding DAPI images are in Extended Data Fig. 12i. Note that regions marked by arrow show a large drop in signal due to the cell-dense cardiac region in the light path. Scale bar 100 µm. **h,** Phase contrast images

focusing on both the cardiac bundle and endothelialized vessel in the view, corresponding TTN-GFP and mRuby fluorescence images. Cardiac contractions displace the tracer beads added to the vascular channel as visualized through a kymograph recorded along a path (see Supplementary Video 16).